Long-range traveling waves of activity triggered by local dichoptic stimulation in V1 of behaving monkeys

Zhiyong Yang, David J. Heeger, Randolph Blake and Eyal Seidemann

J Neurophysiol 113:277-294, 2015. First published 15 October 2014; doi:10.1152/jn.00610.2013

J Neurophysiol 113: 277–294, 2015.
First published October 15, 2014; doi:10.1152/jn.00610.2013.

Long-range traveling waves of activity triggered by local dichoptic stimulation in V1 of behaving monkeys

Zhiyong Yang,[1] David J. Heeger,[2] Randolph Blake,[3,4] and Eyal Seidemann[5]

[1]*Brain and Behavior Discovery Institute, James and Jean Culver Vision Discovery Institute, and Department of Ophthalmology, Georgia Regents University, Augusta, Georgia;* [2]*Department of Psychology and Center for Neural Sciences, New York University, New York, New York;* [3]*Vanderbilt Vision Research Center and Department of Psychology, Vanderbilt University, Nashville, Tennessee;* [4]*Brain and Cognitive Sciences, Seoul National University, Seoul, South Korea; and* [5]*Center for Perceptual Systems and Departments of Psychology and Neuroscience, University of Texas, Austin, Texas*

Submitted 27 August 2013; accepted in final form 8 October 2014

Yang Z, Heeger DJ, Blake R, Seidemann E. Long-range traveling waves of activity triggered by local dichoptic stimulation in V1 of behaving monkeys. *J Neurophysiol* 113: 277–294, 2015. First published October 15, 2014; doi:10.1152/jn.00610.2013.—Traveling waves of cortical activity, in which local stimulation triggers lateral spread of activity to distal locations, have been hypothesized to play an important role in cortical function. However, there is conflicting physiological evidence for the existence of spreading traveling waves of neural activity triggered locally. Dichoptic stimulation, in which the two eyes view dissimilar monocular patterns, can lead to dynamic wave-like fluctuations in visual perception and therefore, provides a promising means for identifying and studying cortical traveling waves. Here, we used voltage-sensitive dye imaging to test for the existence of traveling waves of activity in the primary visual cortex of awake, fixating monkeys viewing dichoptic stimuli. We find clear traveling waves that are initiated by brief, localized contrast increments in one of the monocular patterns and then, propagate at speeds of ~30 mm/s. These results demonstrate that under an appropriate visual context, circuitry in visual cortex in alert animals is capable of supporting long-range traveling waves triggered by local stimulation.

dichoptic stimuli; traveling wave; visual cortex

THE VISUAL CORTEX IS A HIGHLY interconnected, excitable neural network within which local activity could, in principle, instigate traveling waves of activity that spread via regenerative processes from their point of origin to distal locations. Indeed, it has been suggested that this kind of spreading plays important roles in dynamical aspects of visual perception (Sato et al. 2012). However, physiological evidence for spreading waves of neural activity within primary visual cortex (V1) is mixed, with some studies purporting to see spreading activation to localized stimulation (Benucci et al. 2007; Grinvald et al. 1994; Jancke et al. 2004), whereas others attribute that spread to population gain control, not genuine spatiotemporal waves of activity (Sit et al. 2009).

We have previously used voltage-sensitive dye imaging (VSDI) in V1 of awake, fixating monkeys to measure responses to a small stimulus (Sit et al. 2009), and we found that the responses do not extend beyond the region predicted, based on the size of the subthreshold cortical point image (Palmer et al. 2012). Furthermore, the responses began to rise approximately simultaneously over the entire active region but reached their peak more rapidly at the center (Sit et al. 2009). The near-simultaneous onset of responses is inconsistent with a traveling wave that spreads through the cortex at slow speeds. Instead, the differences in the dynamics across space can be explained by spatial differences in local gain that are implemented by a population gain-control mechanism operating simultaneously over the entire active region (Sit et al. 2009). These results cast doubt on the previous reports of stimulus-evoked traveling waves of activity in V1.

In considering this controversy (which we return to in DISCUSSION), we wondered whether the studies published to date have used stimulus conditions appropriate for revealing the existence and properties of network circuitry promoting spreading activation. All of those studies have used isolated, local visual stimulation within an otherwise unstructured visual field to look for putative traveling waves of neural activity. Perhaps, we reasoned, the existence of traveling waves depends on the presence of spatial structure in the visual image and hence, spatially distributed neural activity within the retinotopic map to serve as a carrier for traveling waves. The interconnected neural circuits of the visual cortex, in other words, may be optimized to support spatiotemporal interactions among the representations of multiple image features (i.e., promote global perceptual organization over space and time). The simple, localized stimuli used in the earlier studies may have been ineffective at revealing the dynamics of such circuitry.

One promising candidate for stimuli that may facilitate the promotion of traveling cortical waves includes dichoptic stimuli, where the two eyes view dissimilar monocular patterns. Such stimuli can generate binocular rivalry, a phenomenon characterized by unpredictable fluctuations in visual perception (Blake and Logothetis 2002). When viewing dichoptic stimuli, observers typically perceive smooth transitions in dominance, as one rival stimulus replaces the other in visual awareness. These orderly transitions in perception are particularly conspicuous when viewing large rival patterns whose features have a global configuration. With these kinds of stimuli, one perceives traveling waves in which the visibility of one pattern emerges locally and spreads smoothly and progressively as it renders the other pattern invisible. Ordinarily, these perceptual traveling waves arise spontaneously and spread unpredictably, but the origin and onset of the waves can be controlled experimentally by use of a "trigger," i.e., a brief, local increase in the contrast of the perceptually invisible stimulus (Wilson et al.

Address for reprint requests and other correspondence: E. Seidemann, Center for Perceptual Systems and Depts. of Psychology and Neuroscience, Univ. of Texas, Austin, TX 78712 (e-mail: eyal@austin.utexas.edu).

2001). This trigger procedure allows the measurement of these traveling waves psychophysically. Traveling-wave speed in the cortex was estimated from the psychophysical measurements by using measurements of the cortical magnification in human V1; although varying in speed among observers and with different stimulus configurations, the waves averaged 22 mm/s (Wilson et al. 2001).

These perceptual traveling waves during binocular rivalry suggest the existence of neural waves of cortical activity propagating at speeds much slower than conduction speeds of horizontal axons and extending over distances that far exceed the length of direct horizontal connections. Indeed, it is tempting to hypothesize that these emerging perceptual waves are mediated by a slow, multisynaptic, regenerating process that generates neural activity that can travel over large distances in the cortex. Brain-imaging studies in humans have documented the spread of cortical activity within retinotopically defined areas in early visual cortex, with these cortical activity waves following a time course that mirrored the perceptual waves during rivalry, with an estimated speed that averaged ~20 mm/s (Lee et al. 2005, 2007). Those brain-imaging results, although compelling, are constrained by the limited spatial and temporal resolution of functional MRI (fMRI) and moreover, are subject to alternative interpretations, because the neural basis of the blood-oxygen level-dependent signal is under debate (Bartels et al. 2008; Heeger and Ress 2002; Lauritzen 2005; Logothetis and Wandell 2004; Sirotin and Das 2009).

Here, we used VSDI to test for traveling waves in macaque V1 in response to dichoptic stimuli with a local contrast increment (trigger). Among currently available neurophysiological techniques, VSDI is the only one that allows simultaneous monitoring of neural activity across a large cortical area at both high spatial and high temporal resolutions in alert, behaving primates (Grinvald and Hildesheim 2004). Based on our previous experimental and computational results (Sit et al. 2009), the trigger should produce only a local and transient response and should not initiate an extended and slowly propagating traveling wave in V1. On the other hand, it is possible that under the conditions of dichoptic stimulation, additional mechanisms that are not activated by small, isolated, local stimuli would facilitate the propagation of traveling waves within the extended retinotopic representation of the dichoptic patterns. Our results are consistent with this latter possibility; we observed slow traveling waves in V1 that were time locked to trigger onset and propagated from the retinotopic representation of the trigger at a speed of ~30 mm/s.

MATERIALS AND METHODS

Data Acquisition

Visual stimuli. Stimuli were presented on a 21-in. color display (Sony GDM-F520; 1,024 × 768 pixels), extending over 20.5° × 15.4° of visual angle at a viewing distance of 108 cm, and viewed through a pair of ferroelectric liquid crystal shutters (Displaytech, Longmont, CO) at a refresh rate of 100 Hz (50 Hz/eye). The geometrical configurations of the stimuli are shown in Fig. 1*C*. The stimuli were restricted to an annular region of the visual field (1.5°–2.6° eccentricity), and they all had the same space-averaged mean luminance (30

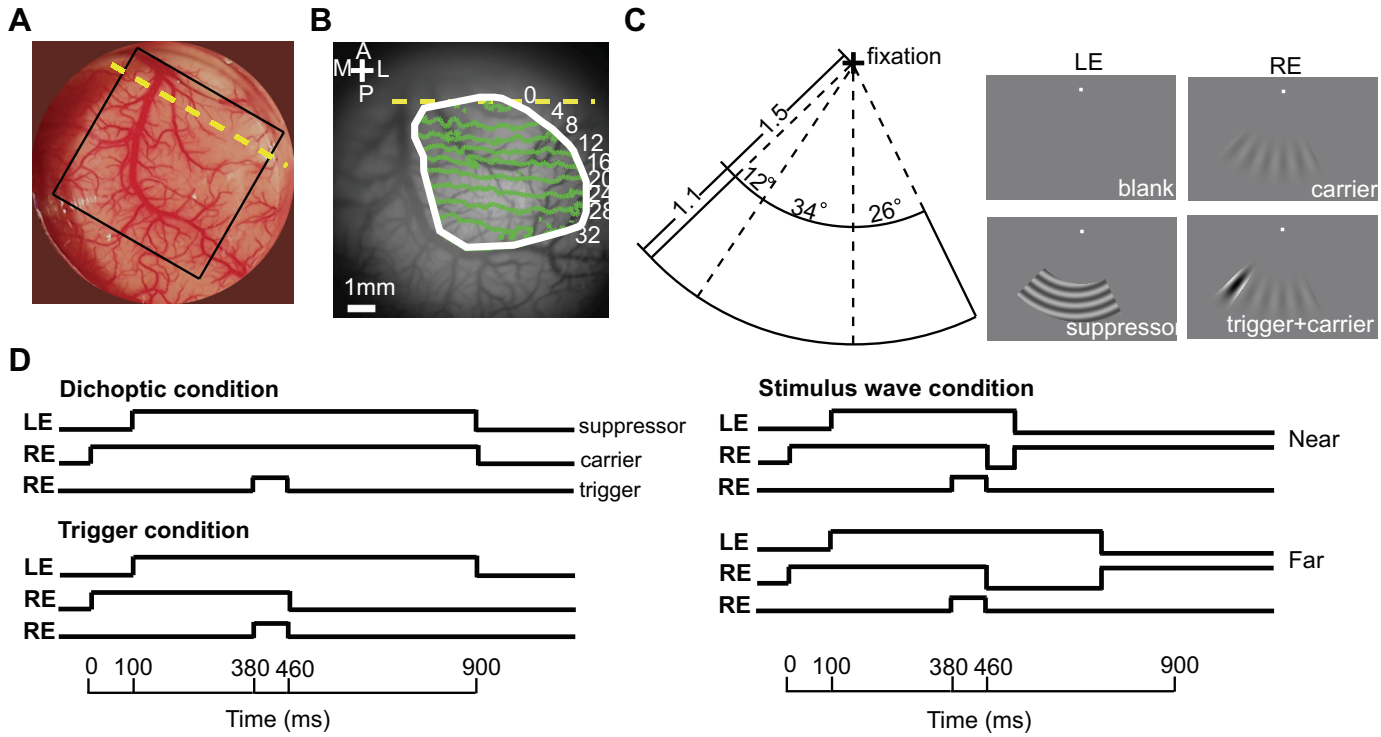

Fig. 1. Imaging chamber, retinotopic map, and visual stimuli. *A*: an imaging chamber over the dorsal portion of the primary visual cortex (V1) and visual area 2 (V2) in the right hemisphere of 1 of the 2 monkeys. Typical imaging area of 14 × 14 mm is indicated by the black square. *B*: retinotopic map of polar angle in degrees relative to the lower vertical meridian. The dashed yellow lines in *A* and *B* delineate the V1/V2 border. The white curve indicates the border of the region of interest (ROI; see MATERIALS AND METHODS). A, anterior; P, posterior; M, medial; L, lateral. *C*: the geometrical configuration of the stimuli and the blank, suppressor, carrier, and trigger plus carrier images. White squares, fixation points. LE, left eye; RE, right eye. *D*: time sequences of stimulus presentations. For the stimulus-wave condition, the stimulus time sequence was different at each location on the screen (see Fig. 3*A*); the panel shows time sequences corresponding to 2 locations (near and far from the location of the trigger).

cd/m^2), equal to the luminance of the background outside of the annulus. We used four classes of visual stimuli: a blank, a high-contrast (40% or 60%, three cycles/degree) spiral suppressor, a low-contrast (10% contrast, 2.25 cycles/degree) radial carrier, and a high-contrast (100%) radial trigger (Fig. 1*C*).

These stimulus components were combined into four conditions: *1*) dichoptic, *2*) trigger, *3*) stimulus wave, and *4*) blank (Fig. 1*D*). The timing of the sequences of presentation is shown in Fig. 1*D* and illustrated as well (see Figs. 3*A*, 5*A*, and 6*A*). The sequence of events in *conditions 1–3* was identical until trigger offset. The carrier appeared first in the right eye for 100 ms. Next, the suppressor appeared in the left eye for 280 ms or 180 ms. When viewed by human observers, the onset of a high-contrast suppressor typically leads to complete perceptual dominance of the suppressor, due to flash suppression (Wolfe 1984). Next, the trigger was presented to the right eye for 80 ms. The trigger spanned 12° of polar angle and was centered 40° or 50° away from the lower vertical meridian (i.e., from the V1/V2 border).

In the dichoptic condition, after trigger offset, the dissimilar carrier and suppressor stimuli were presented simultaneously for 440 or 580 ms for the experiments in *monkey W* and 540 ms for the experiments in *monkey T*.

In the trigger condition, the carrier was turned off at the same time as trigger offset.

In the stimulus-wave condition, immediately after the trigger offset, the carrier was turned off. Next, the suppressor pattern was progressively erased starting at the trigger location at a speed of 160°/s. At the same time, the carrier pattern was progressively redrawn, starting at the trigger location at the same speed and taking over the portion of the stimulus where the suppressor was erased. The perceptual appearance of this sequence of dichoptic presentation was that the low-contrast carrier erased the high-contrast suppressor as a wave starting at the edge of the trigger and progressing rapidly to the lower vertical meridian (see Fig. 3*A*). The speed of the wave in the stimulus-wave condition was chosen to match that perceived by human observers (on average) in the dichoptic condition, measured in a pilot study. To test whether we could use VSDI to detect the wave reliably at different speeds in the stimulus-wave condition, we also ran an experiment in which the wave created in that condition propagated at 80°/s (see Fig. 4).

Voltage-sensitive dye imaging. All procedures were approved by the University of Texas Institutional Animal Care and Use Committee and conform to U.S. National Institutes of Health standards.

Our techniques for optical imaging with VSDI in behaving monkeys have been described elsewhere (Chen et al. 2006, 2008). Briefly, VSDI was performed using an Imager 3001 system (Optical Imaging, Rehovot, Israel) and using the dyes RH-1691 or RH-1838 (Grinvald and Hildesheim 2004; Shoham et al. 1999). The monkey's ECG was monitored continuously, and onset of the data acquisition of the imaging system in each trial was synchronized to the heart beat. Data were collected in two imaging chambers ($\sim$14 $\times$ 14 mm) over the dorsal portion of V1 and V2 in the right hemispheres of two monkeys.

One of the four experimental conditions (dichoptic, stimulus wave, trigger, and blank) was selected randomly for each trial of the experiment. In each imaging trial, the camera collected 110–140 image frames at 100 Hz. Each VSDI image frame had 512 $\times$ 512 pixels with a pixel size of $\sim$0.024 mm $\times$ 0.024 mm (for *monkey W*) or 0.04 mm $\times$ 0.04 mm (for *monkey T*). Note that this low-magnification VSDI is optimized for viewing V1 responses at the retinotopic scale over a relatively large region and does not allow us to see signals at the columnar scale (Chen et al. 2012). Eight to 60 trials were collected for each condition in each experiment.

Eye movements. Eye movements were measured using an infrared eye-tracking device (Dr. Bouis Devices, Karlsruhe, Germany). Each trial began with the monkey acquiring fixation at the center of the monitor for 200–300 ms. The monkey had to maintain fixation within a fixation window (full width 1.6°–2.2°) throughout the trial and for 300 ms after stimulus offset to receive a reward. Trials in which the monkey left the fixation window early were aborted and not analyzed.

Data Analysis

Aligning to retinotopic map and preprocessing. The retinotopic map in each imaging chamber was measured in separate experimental sessions (Yang et al. 2007). For each session of the main experiment, we obtained the retinotopic coordinates corresponding to each location on the cortical surface by aligning the images of the cortical vasculature with those obtained in imaging sessions for retinotopic mapping (Yang et al. 2007).

VSDI signals were preprocessed following standard procedures to remove noise and artifacts (Chen et al. 2006, 2008; Sit et al. 2009). VSDI signals were smoothed with Gaussian filters (σ = 0.055 mm in space; σ = 5 ms in time) to remove high-frequency noise. The smoothed signals were then binned (4 $\times$ 4 pixels) by averaging across the 16 pixels in each bin. The signals in each bin were then normalized by the mean fluorescence, averaged across all trials and frames to remove the effects of uneven illumination and nonuniform staining. The mean time course of the blank condition (averaged over repeated blank trials) was subtracted, separately for each bin, from the time course of the VSDI responses to each trial of each of the other stimulus conditions to remove systematic and repeatable artifacts common to all trials, such as heart-beat artifacts (data acquisition, as noted above, was synchronized to heart beat). Finally, to equalize the baseline response at the beginning of each trial, the mean of the first six imaging frames before stimulus presentation was subtracted from the rest of the time course of that trial, separately for each bin.

ROI selection. A single, closed region of interest (ROI) for each experiment was selected based on an iterative process, in which the following criteria were optimized: *1*) the illumination level at all of the pixels in the ROI was >37% of the maximal illumination in the average of all imaging frames in all conditions; *2*) the mean of the responses (i.e., the relative change in fluorescence emitted by dye molecules) averaged across all pixels in the ROI to the (high-contrast) suppressor was $>8.5 \times 10^{-4}$ (the VSDI response to a high-contrast stimulus is typically $\sim 15 \times 10^{-4}$ in a high-quality experiment); *3*) the signal-to-noise ratio (SNR; mean over SD of response across trials) of the responses to the suppressor averaged across all pixels in the ROI was >5.5.

Experiment inclusion. A total of 15 and 12 experiments was performed in *monkey W* and *monkey T*, respectively. In four experiments in *monkey T*, trials with two trigger locations were interleaved randomly. In these experiments, trials with the two trigger locations were treated as two separate data sets. Two experiments in *monkey W* were excluded due to poor SNR of the VSDI responses to the (high-contrast) suppressor. In addition, to be included in our analysis, ROI height (perpendicular to the V1/V2 border) had to represent at least 20° of polar angle in visual field, and ROI width (parallel to the V1/V2 border) had to be at least 2 mm. Experiments that did not meet the criteria for minimal ROI size were excluded (six in *monkey W* and 10 in *monkey T*). The VSDI responses in the remaining 11 data sets from nine experiments were analyzed for evidence of traveling waves.

Collapsing over isopolar representation and removing outliers. VSDI responses at locations with equal distance from the V1/V2 border (representing isopolar angles) were averaged within the ROI. This yielded a set of response time courses, each one of which corresponded to a different distance in the cortex from the V1/V2 border. For each condition, we computed the mean and SD of the time course at each distance from the V1/V2 border.

A minority of trials was identified as outliers, according to two complementary procedures. For both procedures, we considered only a 500-ms period, starting 10 ms before trigger offset. In the first procedure, we calculated the z-values at each location and time point for each trial using the mean and SD obtained above. We then averaged the z-values at all of the locations, and outliers were defined

as individual trials, in which the average absolute z-value was >3.5 at any time point. In the second procedure, we calculated the Fourier transform of the average time course at all locations. We then obtained z-values of the Fourier amplitudes, and outliers were defined as trials in which the absolute z-value was >4 at any frequency. Fewer than 5% of the total number of trials was excluded, based on one or both of these criteria. The removal of these outlier trials minimized the impact of unidentified and/or uncontrollable mechanical oscillations that occurred in some experimental sessions. After these outliers were removed, the VSDI response time courses were averaged across trials, separately for each stimulus condition.

Fitting traveling waves. To identify patterns of neural activity consistent with a traveling wave propagating in the direction normal to the V1/V2 border (corresponding to the polar direction in the visual field), we developed a spatiotemporal model of the VSDI signals at locations spanning the cortical region from the representation of the trigger to the V1/V2 border (Fig. 2), after collapsing cortical locations over the direction parallel to the V1/V2 border (see above). We analyzed the VSDI signals during a 500-ms-long interval, starting 10 ms before trigger offset. The VSDI response during this period was assumed to be equal to the sum of five spatiotemporal components, one that reflects the traveling wave and four additional components that reflect different features of the VSDI responses.

The first component captured the traveling wave, which in the case of the stimulus wave, was due to the sequential replacement of the high-contrast mask by the low-contrast carrier. There was a clear drop in the VSDI signal after trigger offset (Fig. 2*A*). The drop occurred first at locations closest to the trigger and was progressively delayed as the distance from the representation of trigger increased. This progression appears as a prominent diagonal in the space-time plot (Fig. 2*A*). We modeled this drop in VSDI response at each location as a descending sigmoid function and assumed that the start time of the sigmoidal drop propagated at a constant speed in the cortex (see Table 1). The fitted traveling-wave component and its corresponding space-time plot are shown in Fig. 2*C*.

The second component captured the direct response to the trigger, which was modeled as the combination of rising and falling sigmoid functions in time and a Gaussian function in space (Fig. 2*D*).

The third component was a rise that preceded the drop in the response in the stimulus-wave condition (Fig. 2*E*). The rise was assumed to propagate at the same speed as the descending traveling wave. This rise captured possible effects of contrast gain-control mechanisms (see RESULTS).

The fourth and fifth components were designed to capture slow variations in VSDI signals that could result from neural adaptation and residual sources of non-neural noise that were not removed completely by averaging over repeats (Fig. 2*F*). These slow variations were captured by two linear trends: one before and one after the start of the descending traveling wave.

The model was fitted simultaneously to VSDI results from all three stimulus conditions: stimulus wave, dichoptic, and trigger. Several constraints were imposed on the components of the model. *1*) For all stimulus conditions, the time point at which the descending sigmoid dropped by 5% from its maximum value was constrained to travel at a constant speed on the cortical surface. The speed could be positive (propagating from the representation of the trigger toward the V1/V2 border) or negative (propagating in the opposite direction). The constraint of constant-speed propagation was removed in one version of the analysis (see below). *2*) Because the stimuli were identical in the three conditions before trigger offset, the trigger-evoked component was constrained to be the same for the three stimulus conditions in the same experiment. *3*) For the stimulus-wave condition, the time point at which the rising sigmoid reached 95% of its maximum value was constrained to travel at the same speed as the descending sigmoid function, and the time point at which the rising sigmoid reached 95% of its amplitude was not later than the time point at which the descending sigmoid dropped by 5% from its maximum value. These constraints were adopted because the spatial propagations of the rising and descending sigmoids were both assumed to be evoked by the traveling wave. *4*) The two linear trends were constrained to meet at the time point at which the descending sigmoid dropped by 5% from its maximum value. Additional constraints, as well as equations for each of these components, are listed in Table 1.

With these constraints, the time courses at all locations for the three conditions were fitted simultaneously using the nonlinear fitting routines in MATLAB. We fitted the time courses multiple times for a set of fixed values of wave-initiation times (the time at which the amplitude of the descending sigmoid, at the location closest to the representation of the trigger, dropped by 5%) in steps of 2.5 ms and chose the best fit. The times reported in Table 2 were obtained by extrapolating the initiation times to the location corresponding to the center of the trigger. The other parameters were allowed to vary during the fitting procedure subject to the constraints listed in Table 1.

After completing the fitting, we refitted the data while dropping the constraint that the descending sigmoid function traveled at a constant speed on the cortical surface but holding fixed the values of all of the other parameters. These results are indicated by the white dashed curves in the space-time plots from individual experiments (e.g., see Fig. 3*D*).

We also tried variants of the model in which we removed one or more components and/or altered the constraints. These modified models were unable to detect and measure correctly the waves in the stimulus-wave condition, suggesting that all five model components and the associated constraints were needed to capture the spatiotemporal dynamics of the VSDI signals in the stimulus-wave condition.

Statistics

To evaluate the reliability of the VSDI responses, we resampled trials from the same condition within each data set (with replacement) 2,000 times, calculated the mean time courses, and fitted the data, as described above using a set of fixed values of wave-initiation times (in steps of 10 ms). By combining the bootstrap samples from all data sets, we obtained the distributions of the estimated speeds (see Fig. 10, *A* and *B*) and computed the median, the mode, and the 25th and 75th percentiles of speed, drop time, and drop amplitude (Table 2).

To evaluate the statistical significance of the traveling waves, we computed for each bootstrap sample in each data set and stimulus condition the inverse of speed (1/speed; in s/mm). We performed the calculations with 1/speed instead of speed, because the speed corresponding to the trigger condition was hypothesized (a priori) to be infinite (i.e., the drop was hypothesized to occur simultaneously over space); as hypothesized, the bootstrap distribution of average speed for the trigger condition was poorly sampled with long tails out to very large positive and negative values, whereas the distribution of 1/speed was, as hypothesized, concentrated near zero. In this format, a positive value of 1/speed signifies occurrence of a traveling wave from the representation of the trigger toward the V1/V2 border; a negative value signifies occurrence of a traveling wave from the V1/V2 border toward the representation of the trigger; and a value of zero, corresponding to a vertical space-time plot, denotes the absence of a traveling wave. We averaged the 1/speed values for each bootstrap sample across all data sets from one animal and repeated this procedure 2,000 times to obtain bootstrap histograms of the average 1/speed (see Fig. 10, *C* and *D*). In the trigger condition, we expected to see no consistent descending wave or a small and nearly instantaneous drop (corresponding to infinite speed; i.e., 1/speed = 0) shortly after the carrier was turned off (at the same time as trigger offset). Consistent with this expectation, the distribution of average 1/speed in the trigger condition was centered on zero in both monkeys (see Fig. 10, *C* and *D*). If reliable traveling waves were triggered in the stimulus-wave and dichoptic conditions, then we would expect to obtain statistically reliable, positive 1/speed values. The statistical significance of the traveling wave in each condition was therefore

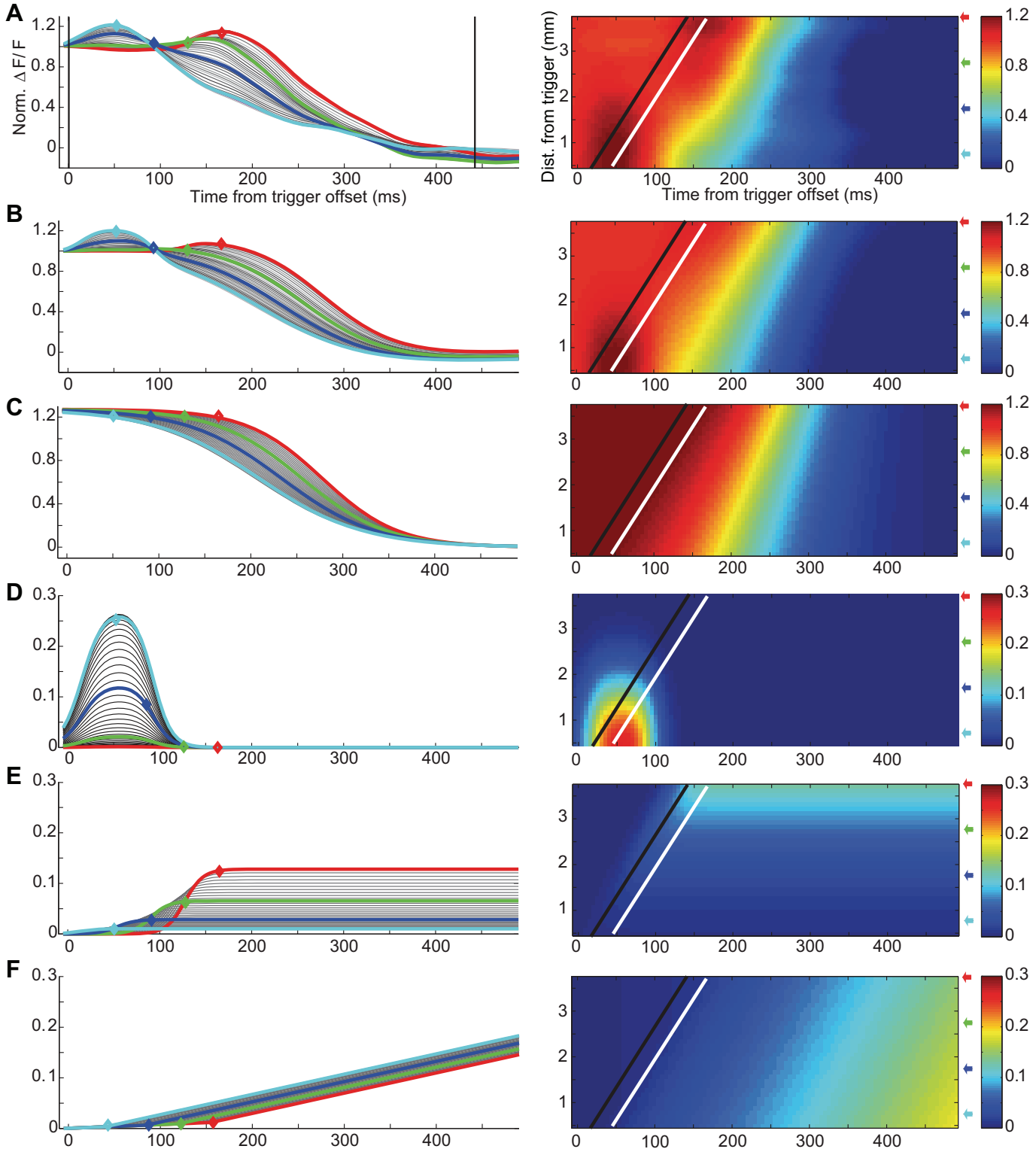

Fig. 2. Fitting the voltage-sensitive dye imaging (VSDI) signals in the stimulus-wave condition. *A*: normalized (Norm.) VSDI responses; grand average of the stimulus-wave condition of all of the data sets acquired in *monkey W*. The vertical lines indicate the time of the trigger offset and the time of stimulus offset. ΔF/F, fractional change in fluorescence. *B*: fitted VSDI responses, using a model with the 5 components shown in *C–F*. *C*: traveling-wave component; *D*: component corresponding to direct trigger-evoked response; *E*: rising sigmoid component; *F*: 2 linear-trend components. *Left*: time courses of the VSDI responses from 10 ms before the trigger offset to 490 ms after the trigger offset and at locations from the cortical representation of the trigger to the V1/V2 border. Cyan traces, locations closest to the trigger; blue, green, and red traces, increasing distance from the representation of trigger. *Right*: space-time plots of the time courses shown on the *left*. The vertical axes show the distance (Dist.) from the trigger location. Colored arrows indicate the cortical locations of the thick-colored traces plotted in the *left*. White lines, locations at which the fitted traveling-wave component of the VSDI responses dropped by 5%; black lines, propagation of the stimulus wave projected to the cortical surface, specifically, the time of transition from the suppressor to the carrier at each location based on the retinotopic map (with no additional delays).

Table 1. *Parameters, constraints, and equations of the wave components*

	Symbols and Equations	Descriptions and Constraints
Descending sigmoid function (F)	t, t_{50}, τ_0, k_τ, u_0, d, d_{50}, d_c	t, time; t_{50}, 50% time point; τ_0, time constant; k_τ, rate of time constant; u_0, amplitude at the V1/V2 border; d, distance to the V1/V2 border; d_{50}, 50% distance point; d_c, distance constant
	$f_1 = \frac{u_0}{1+e^{[(d-d_{50})/d_c]}}$	The time point at which the sigmoid dropped by 5% was constrained to travel at a constant speed on the cortical surface.
	$f_2 = \frac{1}{1+e^{[(t-t_{50})/(\tau_0+k_\tau d)]}}$	VSD amplitude was a sigmoid function of the distance to the V1/V2 border.
	$F = f_1 f_2 + (1 - u_0)$	
Response to trigger (R)	t, d, A, μ, σ, g_τ, g_{50}, h_τ, h_{50}	A, amplitude; μ, mean; σ, SD; g_τ, time constant; g_{50}, 50% time point; h_τ, time constant; h_{50}, 50% time point
	$r_1 = Ae^{[-0.5(d-\mu)^2/\sigma^2]}$	The response was a combination of a rising and a falling sigmoid function in time and a Gaussian function in space.
	$r_2 = 1 + e^{[(t-g_{50})/g_\tau]}$	It was the same in the 3 conditions, and all of the parameters were independent of space.
	$r_3 = 1 + e^{[(t-h_{50})/h_\tau]}$	
	$R = \frac{r_1}{r_2 r_3}$	
Rising sigmoid function	t, a_{50}, a_τ, a_u	a_{50}, 50% time point; a_τ, time constant; a_u, amplitude
	$\frac{a_u}{1+e^{[(t-a_{50})/a_\tau]}}$	It was present only in the stimulus-wave condition.
		There were no constraints on a_{50}, a_τ, and a_u.
		The time point at which the sigmoid reached 95% was constrained to travel at a constant speed on the cortical surface, and the speed was the same as the descending sigmoid function.
First linear trend	K_1, t_m	K_1, slope; t_m, time at which the 2 linear trends met
	$K_1 t$, t $< = t_m$	It was shared by the 3 conditions, and the slope was independent of space.
Second linear trend	K_2, t_m	K_2, slope
	K_2(t $- t_m$), $t > t_m$	It was different in the 3 conditions.
		The slope was independent of space.
		The 2 linear trends met at the time point (t_m), at which the descending sigmoid dropped by 5%.

V1, primary visual cortex; V2, visual area 2; VSD, voltage-sensitive dye.

assessed based on the proportion of average 1/speed with positive values. One minus this proportion provided a one-tailed P value for the statistical significance of 1/speed being positive. In addition, to assess whether the difference between the average 1/speed in the dichoptic and trigger conditions was significant, we converted average 1/speed back to speed, took the absolute value, and determined the proportion of bootstrap samples for which the estimated absolute speed in the trigger condition was higher than the estimated absolute speed in the dichoptic condition. One minus this proportion provided a two-tailed P value for the statistical significance of the difference in speed.

Analysis of Eye Movements

To examine the statistics of eye movements in the three stimulus conditions, we estimated the speed of eye movements along the direction normal to the radial axis of the trigger, within 500 ms after the trigger offset in each trial (Table 3). We used a t-test to determine if there were significant differences in both the mean and peak speeds of eye movements in the three stimulus conditions.

RESULTS

The primary goal of the current study was to determine if traveling waves of activity spread over extended regions in V1 of fixating monkeys as they viewed dissimilar monocular stimuli. To address this goal, we used VSDI in the right hemispheres of two monkeys to measure the spatiotemporal dynamics of V1 population responses during dichoptic stimulation and two control conditions. Before the experiments, the precise retinotopic map in the imaged area of each monkey was measured (Fig. 1*B*) (Yang et al. 2007). These retinotopic maps were then used to tailor the size and location of the visual stimuli for the main experiment (Fig. 1*C*).

On each trial of the "dichoptic condition," the monkey first saw a low-contrast "carrier" pattern presented to the right eye, followed by a high-contrast "suppressor" pattern presented to the left eye (Fig. 1*C*; see MATERIALS AND METHODS for additional details). Shortly thereafter, a brief and local increment in contrast was introduced at the left edge of the carrier pattern (the trigger stimulus; Fig. 1*C*). Our goal was to determine whether the trigger produced a time-locked, slow spreading modulation of VSDI signals within the retinotopic representation of the dichoptic stimuli at sites well beyond the retinotopic representation of the trigger itself, even though the physical stimulation within both eyes remained unchanged following trigger offset.

Before testing for traveling waves of activity in V1 during dichoptic stimulation, we had to address two questions. First, is VSDI in behaving monkeys sufficiently sensitive to reliably measure traveling waves of activity produced by dynamic visual stimuli containing a physical contrast modulation? Only if we can reliably measure traveling waves in V1 to physical contrast waves do we stand a chance of detecting the waves that are bound to be weaker and more variable during dichoptic stimulation. Second, what are the spatial extent and temporal dynamics of V1 responses produced by the onset of the trigger

Table 2. *Statistics of neural activity in the 3 stimulus conditions*

	Median	Mode	25%	75%
Monkey W				
Stimulus wave				
Speed, mm/s	26.4	25.7	23.6	31.2
Drop time, ms	56.4	54	50	74
Drop amplitude	0.74	0.8	0.45	0.85
Dichoptic				
Speed, mm/s	33.2	31.5	26.3	50.8
Drop time, ms	136.5	160	113	160
Drop amplitude	0.59	0.8	0.3	0.8
Trigger				
Speed, mm/s	57.3	58.3	−30	112.4
Drop time, ms	143.1	190	116.5	179
Drop amplitude	0.69	1.4	0.35	1.1
Monkey T				
Stimulus wave				
Speed, mm/s	26.1	23	22.3	32.2
Drop time, ms	100	54	53.5	160.5
Drop amplitude	1.34	1.4	1.15	1.4
Dichoptic				
Speed, mm/s	28.1	28.3	19.2	37.5
Drop time, ms	226.8	178	177.5	244.5
Drop amplitude	0.26	0.1	0.1	0.55
Trigger				
Speed, mm/s	36.7	−4	−40.7	93.3
Drop time, ms	310.4	310	287	383
Drop amplitude	0.21	0.1	0.1	0.35

Median, mode, 25th percentile, and 75th percentile of the speed, drop time, and drop amplitude of the combined bootstrap samples of all of the data sets from the 2 monkeys (7 from *monkey W* and 4 from *monkey T*). Drop time was the time at which the fitted VSD imaging responses dropped by 5% at the cortical location, representing the edge of the trigger. Speed was the estimated speed of the traveling wave on the cortical surface. Drop amplitude was the amplitude of the descending sigmoid function.

under nondichoptic conditions? Under nondichoptic conditions, the trigger should produce a transient increase in responses localized to the retinotopic representation of the trigger and occurring simultaneously within this region (see INTRODUCTION). To demonstrate traveling waves in V1 during dichoptic stimulation, responses should extend over a region that considerably exceeds the direct trigger-evoked response and should propagate from the retinotopic representation of the trigger at slow speeds comparable with those reported perceptually.

To answer the first question, we designed a stimulus sequence termed "stimulus-wave condition." In this condition, following trigger offset, the contrast of the suppressor pattern viewed by the left eye was reduced to zero progressively over space, whereas the contrast of the carrier pattern viewed by the right eye was progressively increased in a complementary fashion (Figs. 1*D* and 3*A*). This sequence of contrast changes progressed in the counter-clockwise direction from trigger location to the opposite edge of the stimulus at a speed of 160°/s (degrees of polar angle/s). This speed was selected, because it matched the average speed reported by human observers during dichoptic stimulation in preliminary tests using identical stimuli.

To address the second question, we designed a stimulus sequence termed "trigger condition." In this sequence, the carrier pattern in the right eye was removed immediately following trigger offset and replaced with a uniform gray stimulus (Fig. 1*D*, and see Fig. 5*A*). These three trial types (dichoptic, stimulus wave, and trigger) and a fourth "blank" condition, in which the stimulus remained uniform gray, were interleaved randomly during each experimental session, and the entire experiment was repeated each time in a slightly different imaging area for each of the two monkeys. We start by describing V1 responses in the stimulus-wave condition.

Consistent Traveling Waves in the Stimulus-Wave Condition

Our first goal was to address two questions. *1*) Is VSDI sufficiently sensitive to detect a traveling wave elicited in V1 in the condition where a real stimulus wave is created? *2*) If so, can the speed of the wave be reliably estimated from the spatiotemporal dynamics of the VSDI response? Our results show that the answers to both of questions are "yes." Figure 3*A* shows the stimulus sequence in the stimulus-wave condition. The imaging chambers were positioned over the dorsal portion of V1 in a region that straddles the V1/V2 border (Fig. 1*A*). In this region of V1, isopolar stimuli are represented by lines parallel to the V1/V2 border (Fig. 1*B*), with the border representing the lower vertical meridian. To obtain reliable measures of the dynamics of V1 responses along the wave's pathway, we averaged the responses within the ROI in the direction parallel to the V1/V2 border, obtaining a set of response time courses, each one of which corresponds to a different distance in the cortex from the V1/V2 border (see MATERIALS AND METHODS).

The results from an example experiment (Figs. 3, *B–E*) show that a clear traveling wave can be seen in the VSDI signals in the stimulus-wave condition. The time courses of the average, normalized VSDI responses at the cortical locations along the wave's expected pathway rapidly reached a plateau ~200 ms after the carrier onset (*time zero* in Fig. 3*B*). The onset of the trigger elicited an additional response at the location representing the edge of the trigger and no response at locations far away from trigger representation. After trigger offset, the carrier gradually replaced the suppressor, starting at the trigger location. The drop in stimulus contrast from the high-contrast suppressor to the low-contrast carrier was accompanied by a clear drop in the VSDI response. Because the drop in stimulus contrast occurred sequentially from the trigger location to the V1/V2 border and because VSDI responses increase monotonically with stimulus contrast (Chen et al. 2006; Sit et al. 2009),

Table 3. *Statistics of eye movements*

	Average Velocity, Visual Angle Per second/Polar Angle Per second	Peak Velocity, Visual Angle Per second/Polar Angle Per second
Monkey W		
Stimulus wave	−0.17 (0.30)/−7.5 (13.2)	−2.73 (6.88)/−120.4 (293.7)
Dichoptic	−0.19 (0.28)/−8.4 (12.3)	−2.94 (6.68)/−129.7 (294.6)
Trigger	−0.19 (0.30)/−8.4 (13.2)	−2.76 (6.61)/−121.7 (291.5)
Monkey T		
Stimulus wave	0.31 (0.33)/13.7 (14.6)	−0.36 (8.82)/−15.9 (389.0)
Dichoptic	0.19 (0.27)/8.4 (11.9)	−2.95 (7.93)/−130.1 (349.7)
Trigger	0.24 (0.30)/10.6 (13.2)	−1.27 (8.45)/−56.0 (372.6)

Mean (SD) of average and peak eye velocities from 7 data sets in *monkey W* and 4 data sets in *monkey T*. Velocity is computed along the direction normal to the radial axis of the trigger within 500 ms after the trigger offset in each trial. Velocities are given in degrees of visual angle/second (*left*) and degrees of polar angle/second (*right*). Negative velocities imply eye movements that brought the trigger away from the lower vertical meridian, which could produce a wave moving away from the V1/V2 border.

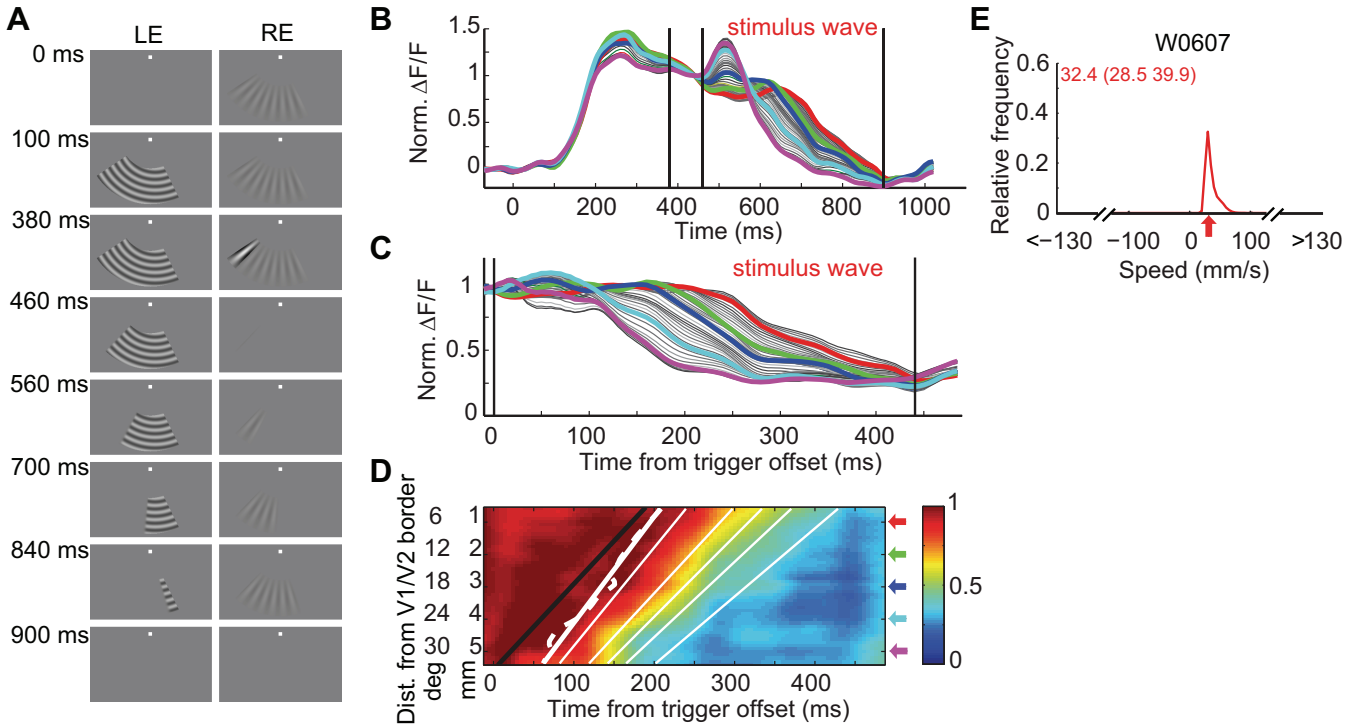

Fig. 3. Traveling wave of neural activity in the stimulus-wave condition in the 1st example experiment. *A*: stimulus sequence. *B*: average normalized time courses of VSDI responses in an example experiment at different distances from the V1/V2 border within the ROI. The VSDI responses before the trigger offset were normalized to 1. The vertical lines indicate the time of the trigger onset and offset and the time of stimulus offset. The thick curves (red, green, blue, cyan, and magenta) represent the time courses of VSDI responses at locations 1, 2, 3, 4, and 5 mm away from the V1/V2 border, respectively, whereas the thin curves indicate time courses in intermediate locations. *Time 0* indicates the onset of the carrier. *C*: traveling-wave component of the VSDI responses after the other fitted components were removed (see Fitting traveling waves in MATERIALS AND METHODS). *Time 0* indicates the offset of the trigger. *D*: space-time plot of VSDI responses shown in *C*. Colored arrows (red, green, blue, cyan, magenta) indicate the locations at 1, 2, 3, 4, and 5 mm away from the V1/V2 border, respectively. Black line, propagation of the stimulus wave projected to the cortical surface; thick, solid white line, locations at which the fitted traveling-wave component of the VSDI responses dropped by 5%; thin, white lines, locations at which the fitted VSDI responses dropped by 10, 30, 50, 70, and 90%; dashed white line, locations at which the fitted traveling-wave component of the unconstrained model dropped by 5%. *E*: the relative frequency of estimated wave speeds of 2,000 bootstrap samples. The median speed and the speed at the 25th and 75th percentiles are indicated in the *top-left* corner. Red arrow, expected speed based on a retinotopic map. Data presented here (and see Figs. 5 and 6) were from the same experiment in *monkey W*, and the trigger was centered at 40° relative to the V1/V2 border.

we expected the drop in the VSDI response to follow this space-time sequence. Indeed, the drop occurred earliest close to the trigger location, progressively later at locations that were farther away from the trigger, and latest at the V1/V2 border.

To analyze the traveling wave quantitatively, we modeled the VSDI responses following trigger offset as the sum of five spatiotemporal components (see MATERIALS AND METHODS; Fig. 2). The first component corresponded to the traveling wave—a sequential drop in the VSDI signal. The second component was the direct trigger-evoked response. The third component was a small, gradual rise in the VSDI response that peaked just before the drop. This rise differed from the response to the trigger in two ways: first, it occurred at locations far away from the trigger, and second, its peak time was progressively delayed from the trigger location to the V1/V1 border. Such increase in response before the drop is consistent with the model proposed by Sit et al. (2009) and most likely reflects the dynamics of the gain-control mechanism implicated in their study. Finally, the fourth and fifth components were two linear trends, one before the drop and one after the drop. These trends reflected slow effects of adaptation and residual, low-frequency variability due to slow fluctuations in the VSDI signal (see MATERIALS AND METHODS).

To determine whether the traveling wave in the stimulus-wave condition accorded with the prediction based on the retinotopic map and to estimate the speed of the traveling wave, we fitted the model to the VSDI response along the wave's pathway. Because the representation of polar angles changes at a nearly constant rate in this region of V1 (Fig. 1*B*), we expected the timing of the drop in V1 responses to be a linear function of distance from the V1/V2 border. Therefore, we fitted the responses with two versions of the model: a constrained model, in which the time of the drop as a function of distance from the V1/V2 border was constrained to fall on a straight line in the space-time plot (assuming a constant-speed wave front), and an unconstrained model, in which the time of the drop was allowed to vary independently at each location (see MATERIALS AND METHODS).

Our results are consistent with a wave that traveled in V1 at a constant speed; the constrained model accounted for 97% of the total variance in the stimulus-wave condition in this experiment. The results from this experiment also demonstrate that the speed of the stimulus in the stimulus-wave condition can be estimated from the speed of the traveling wave in V1. To better visualize the traveling wave, Fig. 3, *C* and *D*, shows the traveling-wave component of the VSDI responses after all of the other fitted components were removed. In this experiment,

the speed of the traveling wave was overestimated slightly. The estimated speed of the traveling wave (Fig. 3*D*) was 29.8 mm/s on the cortical surface. Based on the retinotopic map (Fig. 1*B*) and the rate of change in polar angle as a function of distance in the cortex (6.04° of polar angle/mm), we found that the corresponding speed in the visual field was 179.9°/s, which was slightly higher than the actual speed of the stimulus (160°/s in the visual field, corresponding to 26.5 mm/s on the cortical surface; Fig. 3*D*).

A bootstrap analysis showed that the speed of the stimulus can be estimated reliably from the spatiotemporal dynamics of V1 responses (see MATERIALS AND METHODS). The bootstrapped distribution of estimated traveling-wave speeds in the example experiment (Fig. 3*E*) was narrow, with 25th and 75th percentiles (28.5 and 39.9 mm/s, respectively) close to the expected speed of 26.5 mm/s.

To assess the significance of our assumption that the wave front propagates at a constant speed, we examined the drop times in the unconstrained model (Fig. 3*D*). Specifically, we computed the correlation between the drop times of the constrained and unconstrained models. For the example experiment, the estimated drop times from the unconstrained model were highly correlated with the estimates from the constrained model ($r = 0.99$).

The constrained model provided an excellent fit to the VSDI signals in the stimulus-wave condition for each of the data sets. The model accounted for 99.7% of the total variance in the experiments with *monkey W* ($n = 7$ data sets) and for 99.0% of the total variance in the experiments with *monkey T* ($n = 4$ data sets). Across all experiments in both monkeys, the average correlation coefficient between the timing of the constrained and unconstrained drops was 0.995.

The speed of the stimulus in the stimulus-wave condition was estimated reliably from the spatiotemporal dynamics of V1 responses (see Fig. 10, *A* and *B*). After combining the bootstrap distributions from all experiments in each monkey, the combined distributions were centered on the expected speed, with 25th and 75th percentiles spanning a narrow range of speeds. These results are summarized further in Table 2. The mode of the estimated speed of the cortical wave was 25.7 mm/s in *monkey W* and 23.0 mm/s in *monkey T*, which is very close to the expected speeds (26.5 mm/s in *monkey W* and 19.9 mm/s in *monkey T*). Similarly, Table 2 shows that the estimated drop times and drop amplitudes were narrowly distributed. Results from an additional experiment in *monkey W* with a slower stimulus-wave condition (80°/s) showed that the speed of the cortical wave again closely matched the predicted speed based on the retinotopic map (Fig. 4).

Overall, then, our results demonstrate that the VSDI technique and our analysis methods were sufficiently sensitive to detect traveling waves in V1 of fixating monkeys and to estimate the speed of the wave in the stimulus-wave condition.

No Consistent Traveling Waves in the Trigger Condition

Our next goal was to determine the dynamics and extent of the direct trigger-evoked response in the absence of physical contrast modulation or dichoptic stimulation. Figure 5*A* shows the stimulus sequence in the trigger condition. In this condition, the carrier pattern was turned off at the time of trigger offset, and thus there was neither physical contrast change nor dichoptic stimulation after trigger offset. In addition to the direct trigger-evoked response, we would expect a small drop in the VSDI response shortly after trigger offset, due to the offset of the carrier. This drop should occur at the same time at all cortical locations within the ROI. Given that VSDI responses saturate at low contrasts (Chen et al. 2006; Sit et al. 2009), the drop, due to carrier offset, is expected to be quite small, because the high-contrast suppressor is still present.

Whereas we do not expect to find reliable waves that propagate at slow speeds in this condition, neural responses in the cortex are variable from trial to trial, and these variations can contain spatiotemporal dynamics that may resemble traveling waves [e.g., Nauhaus et al. (2009)]. In addition, various sources of non-neural noise contaminate VSDI measurements (Chen et al. 2006, 2008). Because the number of repeats in each experiment was limited and the magnitude of these

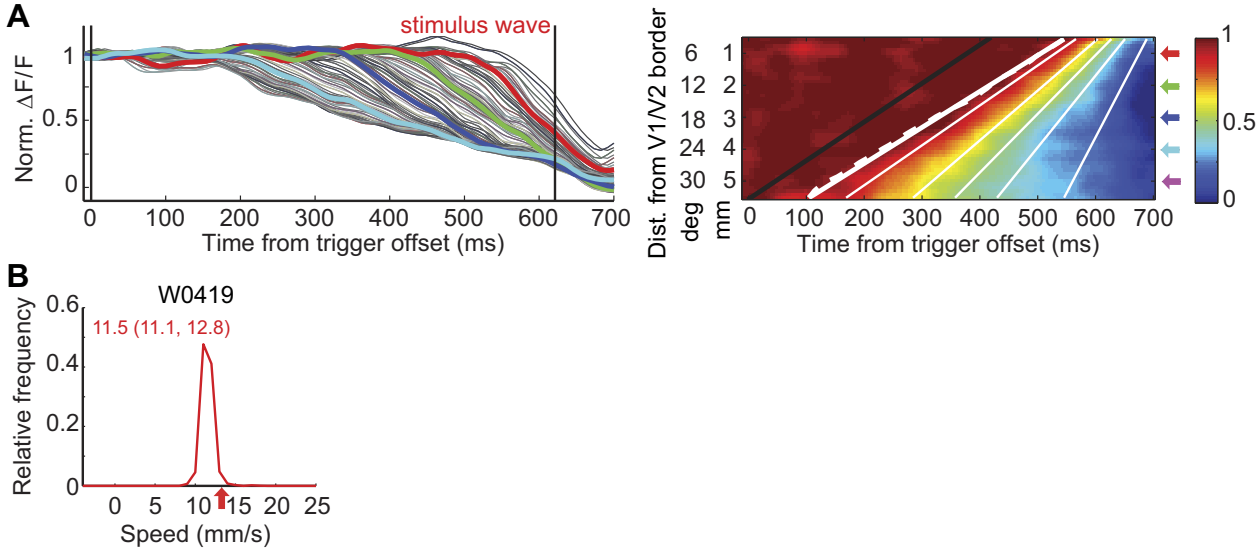

Fig. 4. VSDI responses in the stimulus-wave condition in an experiment where the speed of the wave was 80°/s. *A*: time course and space-time plot (same format as Fig. 3, *C* and *D*, respectively). *B*: relative frequency of estimated wave speeds of 2,000 bootstrap samples (same format as Fig. 3*E*).

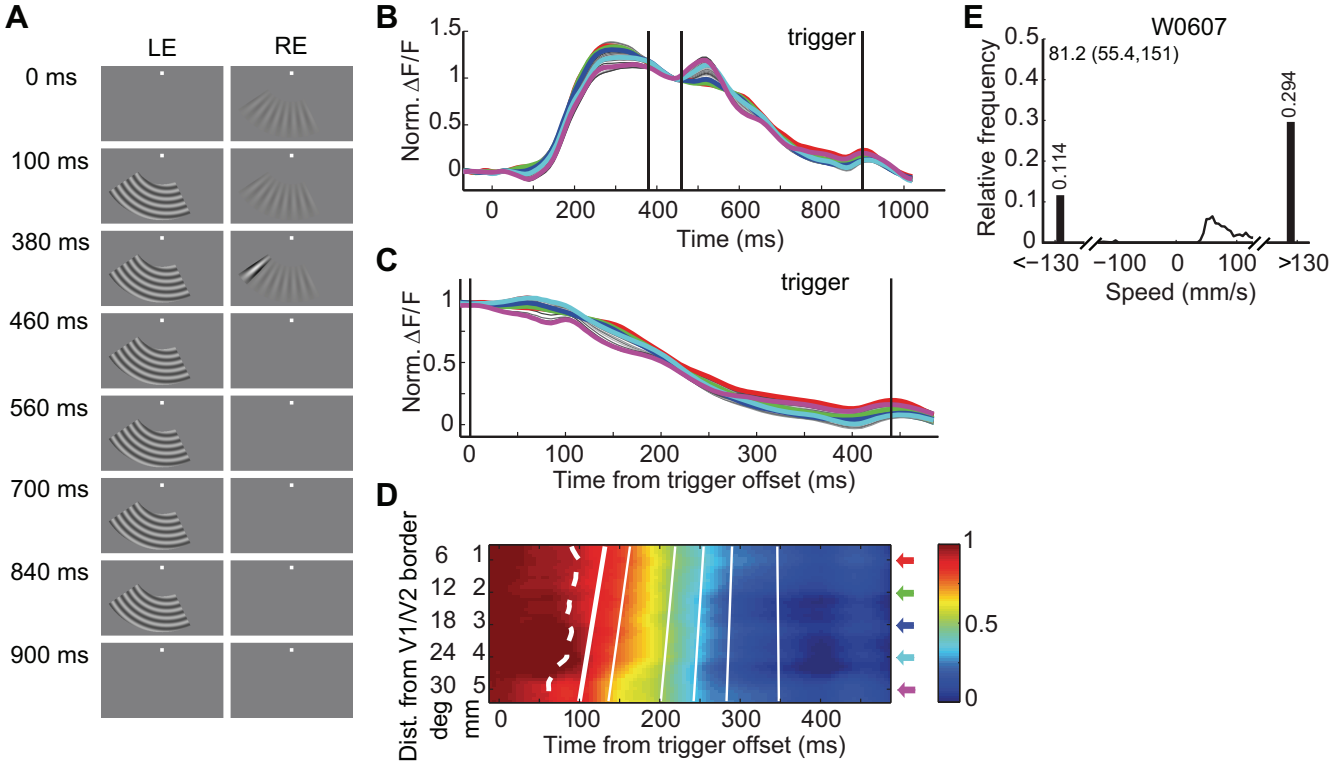

Fig. 5. No traveling wave in the trigger condition in the 1st example experiment (same format as Fig. 3).

variations could have been comparable with the stimulus-evoked responses, averaging across trials might not completely eliminate these sources of variability, and the residual variability could contain spurious, wave-like spatiotemporal dynamics that exceeded the amplitude of the drop due to carrier offset. Our model, therefore, is expected to detect such spurious waves in this condition, but their amplitude should have been lower than in the stimulus-wave condition, and their speed, direction, amplitude, and timing should have been highly variable.

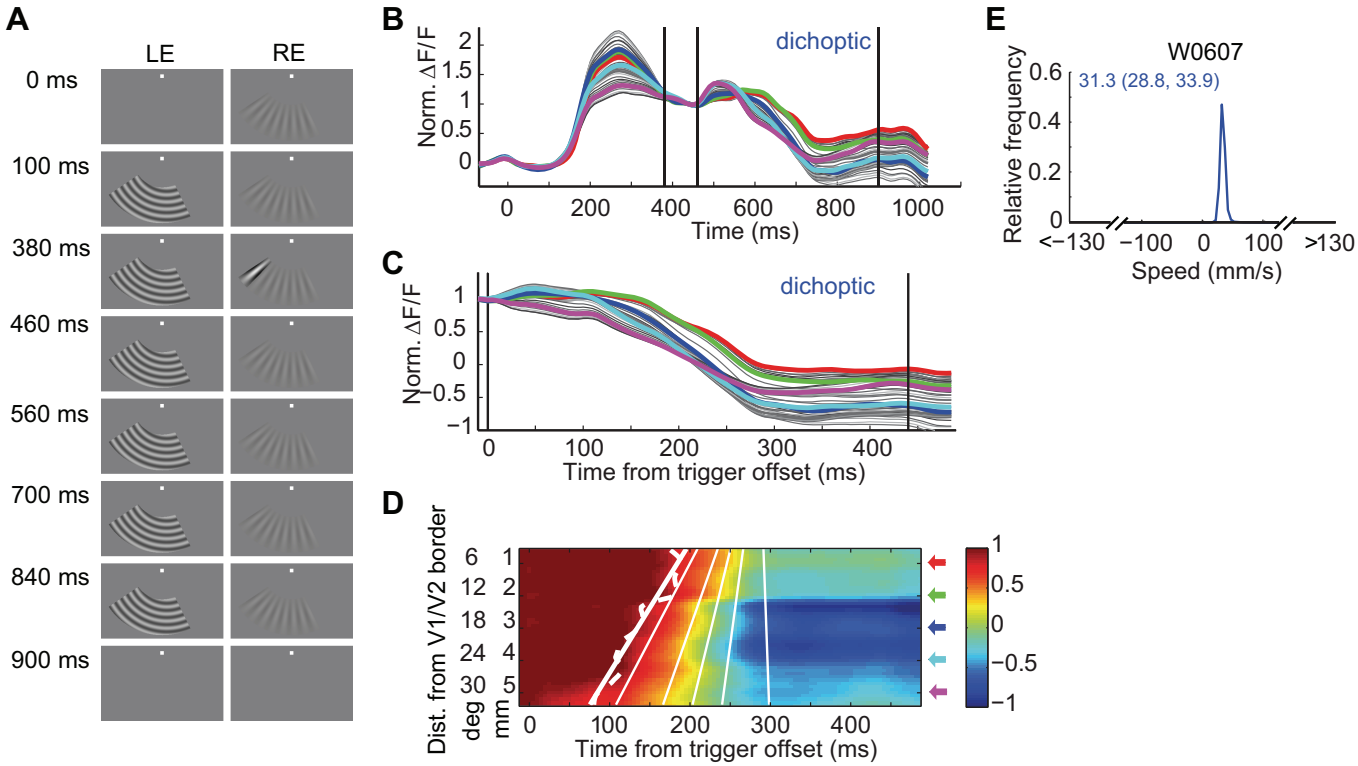

Fig. 6. Traveling wave of neural activity during dichoptic stimulation in the 1st example experiment (same format as Fig. 3).

The trigger condition showed a drop in the VSDI signals after the offset of the trigger and carrier (Fig. 5; results from the same example experiment as in Fig. 3). As in the stimulus-wave condition, the trigger elicited an increase in the VSDI responses at V1 regions corresponding to the trigger location. This direct, trigger-evoked response was local and transient. In addition, ~200 ms after trigger and carrier offset, a delayed drop in the response appeared at nearly the same time at all locations. We fitted these responses using the same procedure used to fit the stimulus-wave data. The constrained fits accounted for 97% of the total variance in the data in this example. Figure 5, *C* and *D*, shows the traveling-wave component of the VSDI responses after the other fitted components were removed. The estimated propagation speed in this experiment was 63.8 mm/s.

In contrast to the consistent traveling wave in the stimulus-wave condition, responses in the trigger condition were highly variable within and across experiments. Figure 5*E* shows the bootstrap distribution of estimated speeds in this condition in the example experiment. Consistent with our expectations, the distribution was very broad, and a considerable fraction of the speeds (40.8%) was negative (i.e., traveling from the V1/V2 border toward the trigger location) or >130 mm/s.

The combined results across all data sets in the trigger condition show that no reliable waves were obtained in this condition (see Fig. 10, *A* and *B*). This was assessed further by examining the distribution of 1/speed (expressed in units of s/mm) of the descending drop in the trigger condition (see Fig. 10, *C* and *D*, and see MATERIALS AND METHODS). The distribution of 1/speed was centered on zero in both monkeys, providing further evidence that in this condition, no consistent descending wave (or a small and nearly instantaneous drop) was obtained.

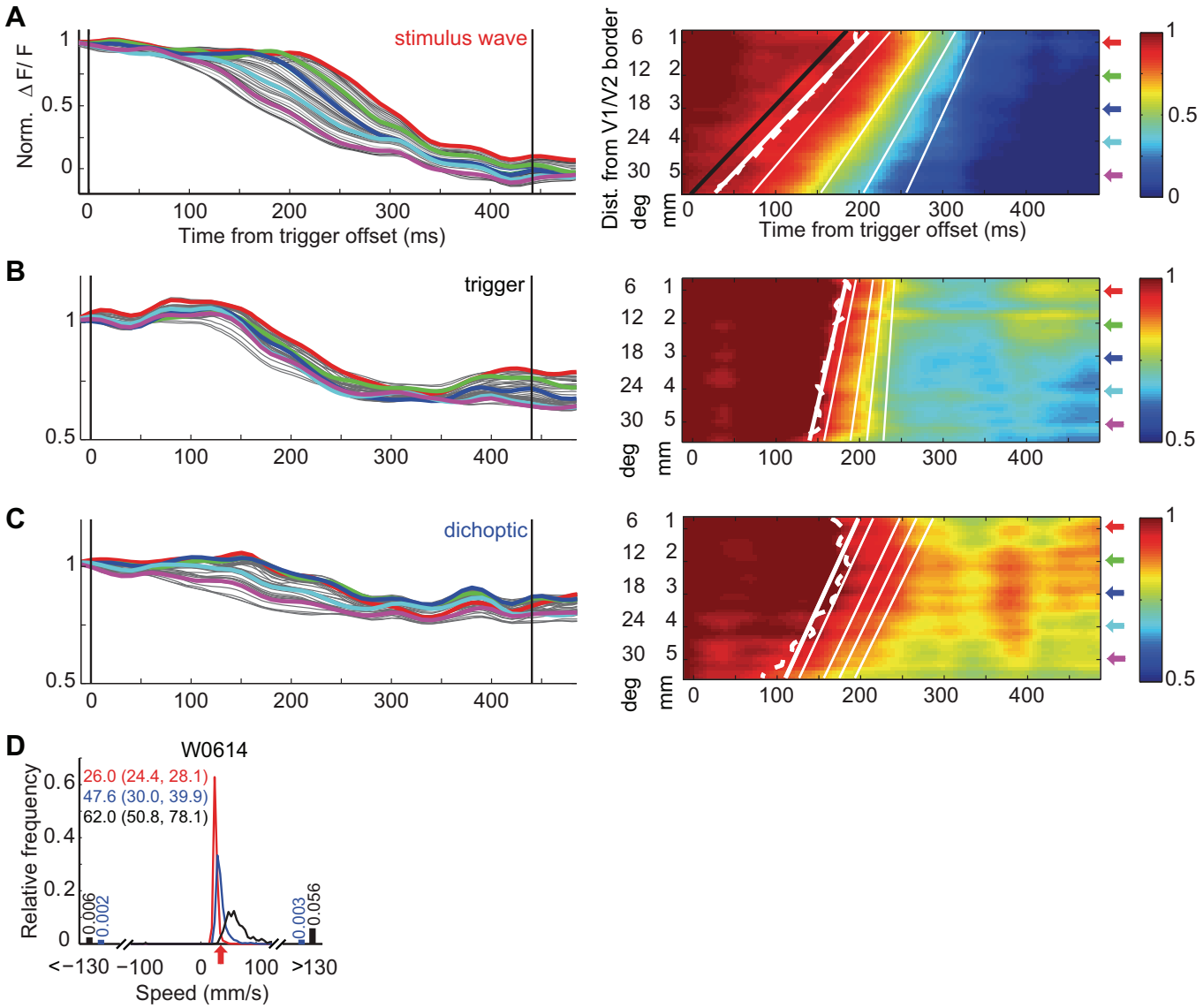

Fig. 7. Second example experiment. *A*: stimulus-wave condition (time course and space-time plot; same format as Fig. 3, *C* and *D*, respectively). *B*: trigger condition. *C*: dichoptic condition. *D*: relative frequency of estimated wave speeds of 2,000 bootstrap samples in each condition. The colored numbers are the median speed (25th percentile, 75th percentile). Red, stimulus-wave condition; black, trigger condition; blue, dichoptic condition. Data were from an experiment in *monkey W*, and the trigger was centered at 40° relative to the V1/V2 border.

The results are summarized further in Table 2. The propagation speeds were highly variable across experiments, and in many cases, the drops in the VSDI signal propagated in the opposite direction (toward the trigger location). In addition, the latency of the drop in the VSDI response was delayed and more variable than in the stimulus-wave condition. Finally, the average amplitude of the drop was smaller and more variable than that in the stimulus-wave condition.

Traveling Waves during Dichoptic Stimulation

Having established that VSDI is sufficiently sensitive to detect traveling waves in V1 in the stimulus-wave condition and that no reliable waves were detected in V1 in the trigger condition, we next examined V1 responses during dichoptic stimulation. In this condition, the carrier and suppressor remained static after trigger offset, maintaining dichoptic stimulation (Fig. 6*A*). If these stimulus conditions evoke traveling waves in V1, then the VSDI signal should drop in amplitude following the trigger onset, and this drop should propagate as a traveling wave similar to that observed in the stimulus-wave condition.

There was a clear traveling wave in the VSDI signals in the dichoptic condition (Fig. 6), similar to the stimulus-wave condition (Fig. 3) and unlike the trigger condition (Fig. 5) from the same example experiment. Shortly after trigger offset, there was a drop in the VSDI signal. As in the stimulus-wave condition, the drop occurred earliest close to the trigger location, later at the locations that were farther away from the trigger, and latest near the V1/V2 border. The sequential drop in the VSDI responses was prominent after removing the other fitted components (Fig. 6, *C* and *D*). The constrained model accounted for 97% of the total variance in the data in this example, and the estimated speed of the traveling wave was 31.1 mm/s, corresponding to a speed of 187.8°/s in the visual field.

Across most experiments in both monkeys, the dichoptic condition generated a traveling wave of neural activity in V1

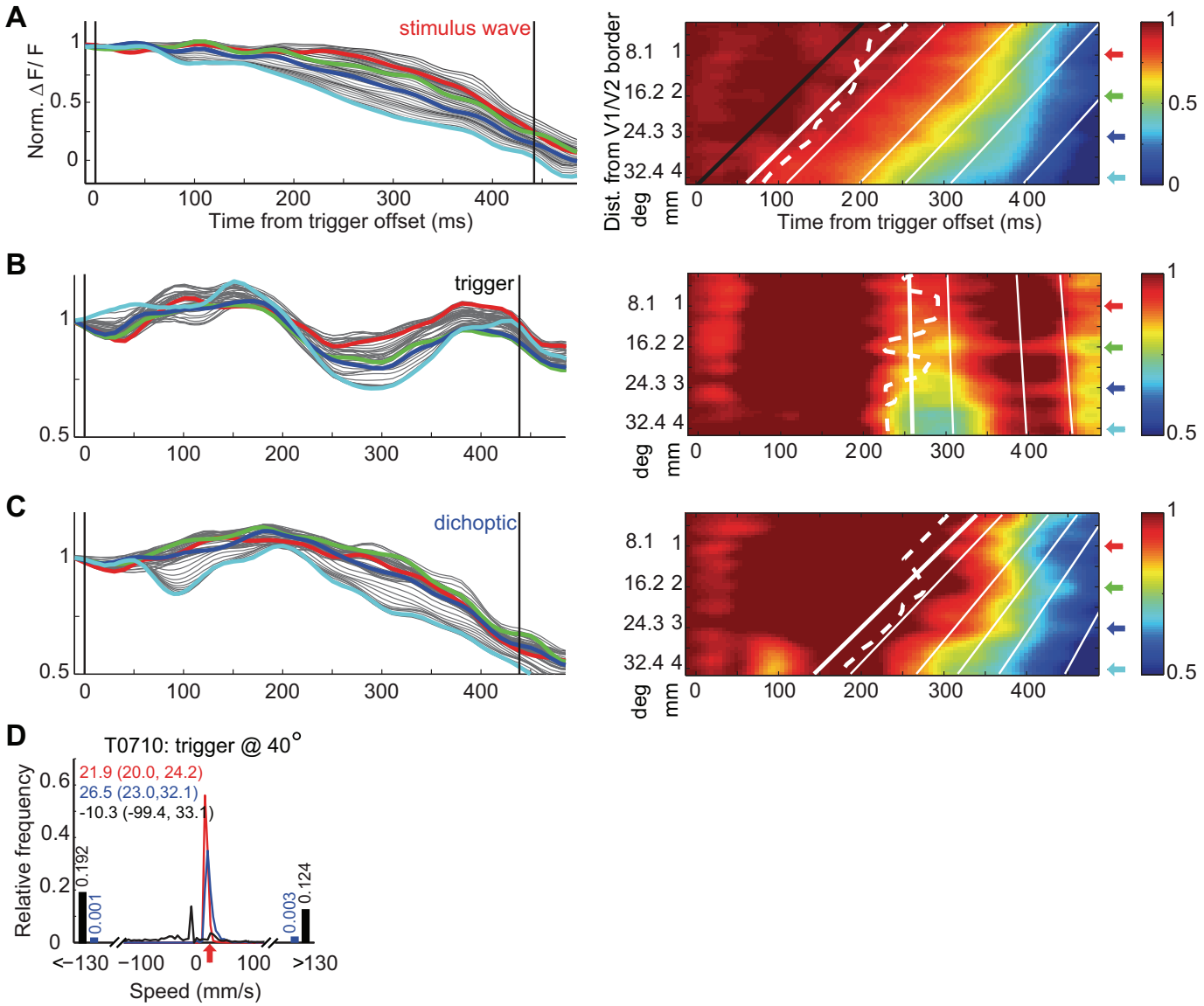

Fig. 8. Third example experiment (same format as Fig. 7). Data were from an experiment in *monkey T*, and the trigger was centered at 40° relative to the V1/V2 border.

that could be detected reliably by VSDI. Figures 7 and 8 show results from two such experiments. However, in some experiments, the analysis failed to detect a reliable traveling wave in the dichoptic condition, and the results were similar to the trigger condition. An example of such an experiment is shown in Fig. 9. In this experiment, the bootstrap distributions for the stimulus-wave condition (Fig. 9*D*) showed a clear and narrow peak around the expected speed, whereas no such peak was observed in the trigger and dichoptic conditions (Fig. 9*D*).

The distribution of estimated speeds in the dichoptic condition contained a clear peak at low positive speeds for both monkeys (Fig. 10, *A* and *B*). These results indicate that a slow traveling wave with speeds comparable with those predicted by psychophysical measurements in humans can be observed in V1 of fixating monkeys. To assess the statistical significance of these results, we examined the distribution of the average 1/speed of the descending drop in the dichoptic condition (Fig. 10, *C* and *D*). The vast majority of the average 1/speed values had positive values (97.45% and 99.65% in *monkeys W* and *T*, respectively), indicating that a reliable, slowly propagating wave was observed in the dichoptic condition in both monkeys.

The combined results across all experiments in each monkey are summarized further in Table 2. The mode of the estimated speeds across all experiments in *monkey W* was 31.5 mm/s, corresponding to a wave of 189.9°/s in the visual field. The mode of the estimated speeds across all experiments in *monkey T* was 28.3 mm/s, corresponding to a wave of 227.6°/s in the visual field.

Comparing Stimulus-Wave, Trigger, and Dichoptic Conditions

The traveling waves in the dichoptic and trigger conditions were statistically different. We used a bootstrap procedure (see Statistics in MATERIALS AND METHODS) to compare the distributions of 1/speed of the descending wave in these two conditions (Fig. 10, *C* and *D*). To do that, we converted average 1/speed back to speed, took the absolute value, and determined the

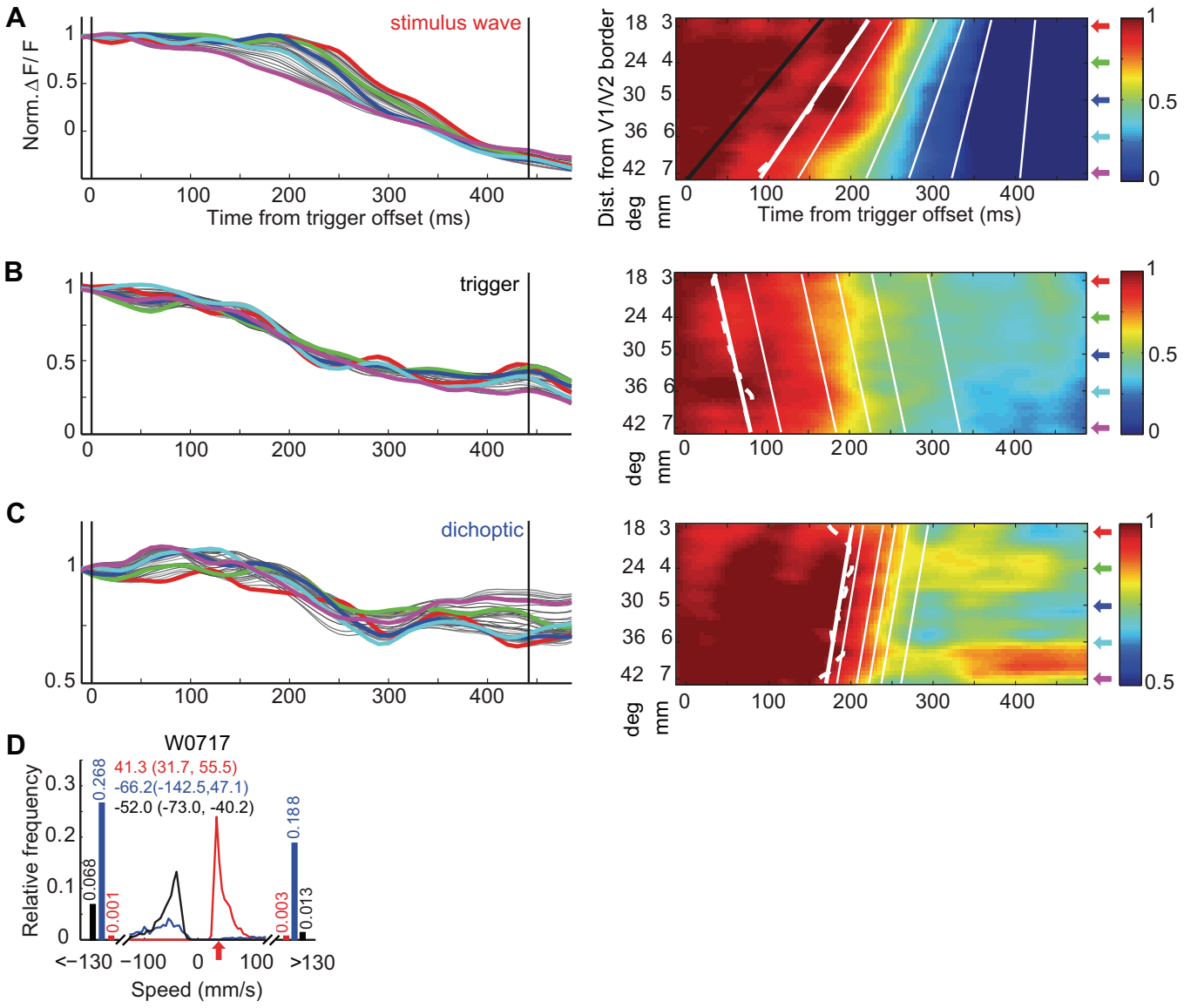

Fig. 9. Fourth example experiment (same format as Fig. 7). Data were from an experiment in *monkey W*, and the trigger was centered at 40° relative to the V1/V2 border.

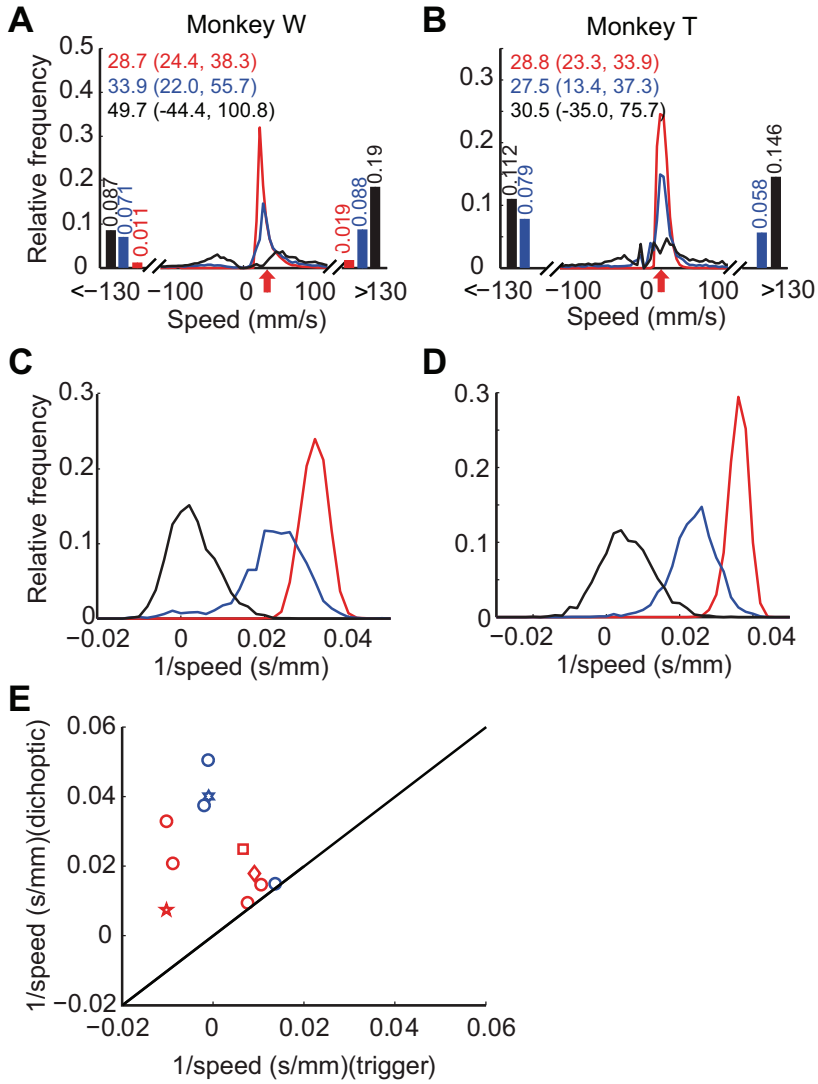

Fig. 10. Distributions of estimated wave speeds and significance analysis. *A*: distributions of estimated wave speed in bootstrap samples combined across all 7 data sets in *monkey W*. *B*: distributions of estimated wave speed in bootstrap samples combined across all 4 data sets in *monkey T*. The colored numbers in each panel are the median speed (25th percentile, 75th percentile). Red, stimulus-wave condition; black, trigger condition; blue, dichoptic condition. *C*: distribution of the average inverse of speed (1/speed; expressed in units of s/mm) of the traveling waves in the 3 conditions in the experiments on *monkey W*. *D*: same as C for *monkey T*. *E*: scatter plot of the estimated 1/speed (s/mm) values in the dichoptic condition vs. the trigger condition in all data sets from the 2 monkeys. Red, *monkey W*; blue, *monkey T*; square, example shown in Figs. 5 and 6; diamond, example shown in Fig. 7; hexagram, example shown in Fig. 8; pentagram, example shown in Fig. 9.

proportion of bootstrap samples for which the estimated absolute speed in the trigger condition was higher than the estimated absolute speed in the dichoptic condition. The proportion of bootstrap samples for which the absolute speed during the trigger condition was larger than the absolute speed during the dichoptic condition was 96.3% in *monkey W* and 96.5% in *monkey T*, demonstrating that the incidence of traveling waves was significantly higher during dichoptic compared with trigger condition ($P < 0.05$) in both monkeys. These bootstrap results are also consistent with a simple comparison of the estimated 1/speed in the dichoptic and trigger conditions in all 11 data sets combined across monkeys (Fig. 10*E*). The mean 1/speed was not significantly different from zero in the trigger condition (Wilcoxon signed-rank test, $P = 0.745$). The mean 1/speed was significantly different from zero in the dichoptic condition (Wilcoxon signed-rank test, $P < 0.001$). Finally, mean 1/speed in the dichoptic condition was significantly different from mean 1/speed in the trigger condition (Wilcoxon signed-rank test, $P < 0.001$).

The responses during the dichoptic condition differed from those during the trigger condition in three ways (Table 2). First, the wave speed was significantly slower in the dichoptic condition compared with the almost-instant drop in the VSDI signals produced by the trigger condition (see preceding paragraph). Second, the estimated speed and direction of the traveling wave in the dichoptic condition were more reliable (Table 2; 25th and 75th percentiles) than those in the trigger condition. Third, the median latency of the traveling wave in the dichoptic condition was shorter (on average, by 6.6 ms in *monkey W* and by 83.6 ms in *monkey T*), indicating a tighter link between the trigger offset and the initiation of the wave-like VSDI activities.

The VSDI responses in the dichoptic condition were also different from the responses in the stimulus-wave condition. First, the waves in the dichoptic condition were weaker than the waves in the stimulus-wave condition. The median drop amplitude (i.e., the amplitude of the descending sigmoid function) in VSDI responses after the trigger offset was ~80% of the drop in the stimulus-wave condition in *monkey W* and ~20% of the drop in the stimulus-wave condition in *monkey T* (Table 2). Second, there was greater variability in the estimated speed of the traveling wave. The lower amplitude of the wave could have contributed to the greater variability, simply because the accuracy of the speed measurement depended on the magnitude of the drop in the VSDI signal. Third, the wave had a higher probability of disappearing before it reached the

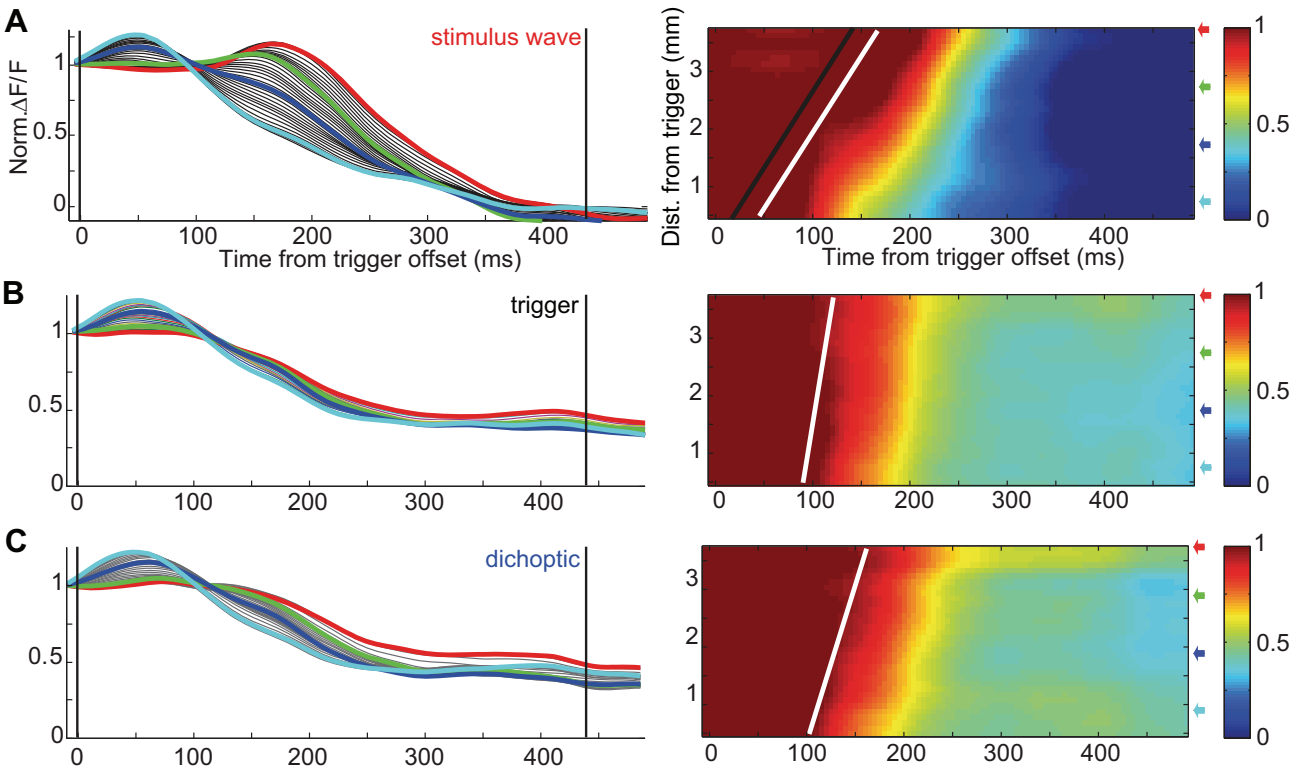

Fig. 11. Grand averages of the VSDI responses in all of the data sets acquired in *monkey W*. *Left*: mean time courses of the VSDI responses from 10 ms before the trigger offset to 490 ms after the trigger offset at locations from the trigger to the V1/V2 border. VSDI responses were averaged across all data sets, after aligning relative to the cortical sites in each experiment that corresponded to the trigger. *Right*: space-time plots of the time courses shown on the *left*. The vertical axes show the distance from the trigger location. Colored arrows indicate the cortical locations of the thick-colored traces plotted on the *left*. *A*: stimulus-wave condition; *B*: trigger condition; *C*: dichoptic condition. White lines, locations at which the fitted traveling-wave component of the VSDI responses dropped by 5%; black line, propagation of the stimulus wave projected to the cortical surface.

V1/V2 border. The sequence of events comprising the dichoptic condition—dichoptic stimulation, followed quickly by a monocular trigger—was tailored to evoke waves that traveled from the trigger location to the V1/V2 border. However, it was sometimes difficult to obtain good staining and illumination near the V1/V2 border. Thus the wave became weaker in both the stimulus-wave and the dichoptic conditions as it approached the V1/V2 border. Since the amplitude of the wave in the dichoptic condition was lower than in the stimulus-wave condition, the wave could have become too weak to be detected in the dichoptic condition, while remaining detectable in the stimulus-wave condition as it approached the V1/V2 border. Finally, in contrast with the stimulus-wave condition, there was usually little or no rise in the VSDI signal before it started to drop in the dichoptic condition.

The grand mean VSDI responses supported the same conclusions (Figs. 11 and 12). As a complementary analysis, we combined all of the data acquired from each animal, averaging the VSDI responses, after aligning the data relative to the cortical sites in each data set that corresponded to the trigger. Clear and robust traveling waves were observed in both monkeys in the stimulus-wave condition (Figs. 11*A* and 12*A*), and the estimated speeds of the waves in these grand averages were similar to the expected speeds, based on the retinotopic map (compare slopes of white and black lines in the *right* panels in Fig. 11*A* and Fig. 12*A*). Similar traveling waves were evident in the dichoptic condition (Figs. 11*C* and 12*C*) but not in the trigger condition (Figs. 11*B* and 12*B*).

Eye Movements Did Not Contribute to Traveling Waves during Dichoptic Stimulation

To determine if systematic eye movements within the fixation window could have contributed to the observed traveling waves in the dichoptic condition, we analyzed several aspects of eye position during the temporal interval in which the traveling waves were observed. To generate a wave-like response in V1 after trigger offset, the eyes would have had to move in a trajectory that was roughly normal to the radial axis of the trigger (Fig. 1*C*). Therefore, we measured the average and peak eye velocity in this direction during the 500 ms after the trigger offset. The values of the average eye velocities were much lower than the speed of the traveling waves in the stimulus-wave and dichoptic conditions (Table 3). Nevertheless, we tested for significant differences between the average and/or peak eye velocity in the dichoptic and trigger conditions in individual experiments. In nine of the 11 data sets, both the average eye velocity and the peak eye velocity were not significantly different between the dichoptic and trigger conditions. Eye movements in the remaining two data sets were inconsistent; peak eye velocities were not significantly different, but average eye velocities were significantly lower in the dichoptic condition than the trigger condition in one experiment and vice versa in the other experiment. We conclude that eye movements within the fixation window were unlikely to have contributed to the traveling wave in the dichoptic condition.

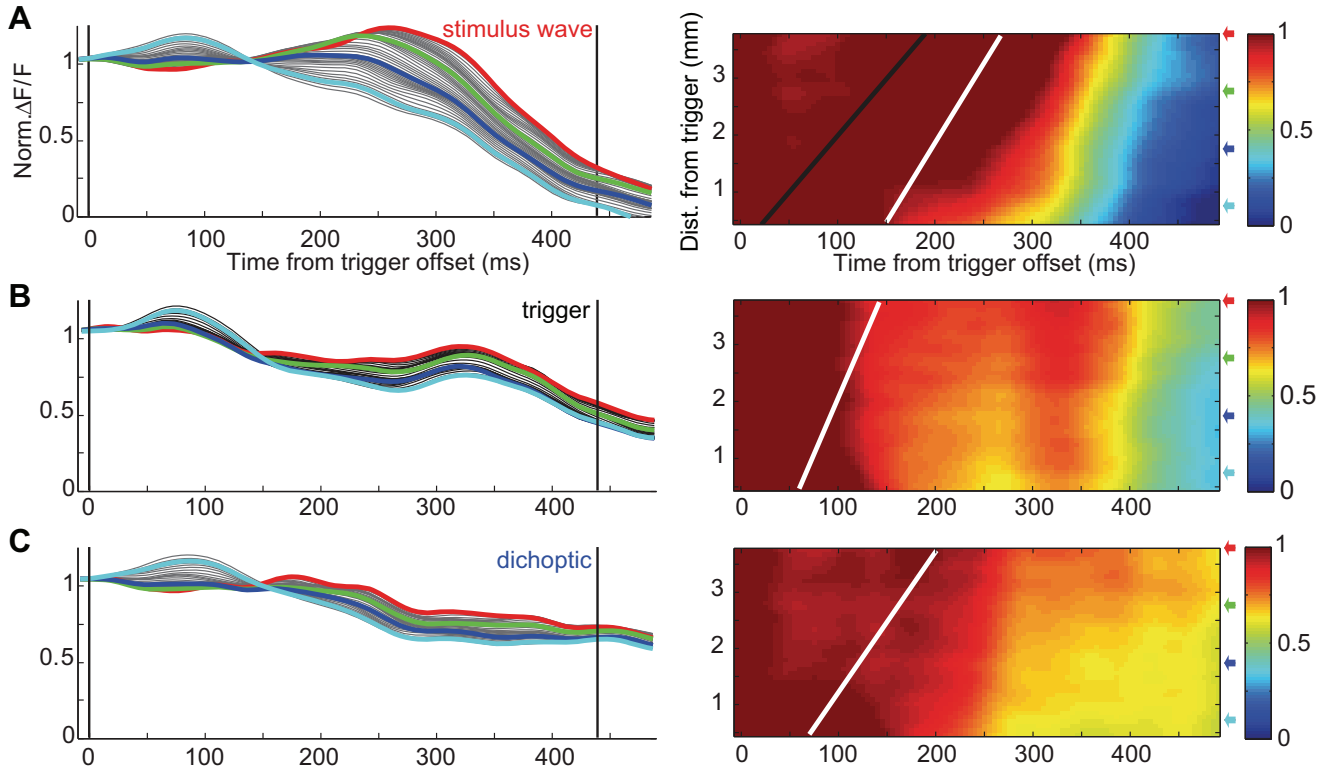

Fig. 12. Grand averages of the VSDI responses in all of the data sets acquired in *monkey T* (same format as Fig. 11).

DISCUSSION

The goal of the current study was to test whether local visual stimulation can trigger long-range traveling cortical waves in V1. Our findings suggest that such waves can be triggered in V1 of awake, fixating macaque monkeys under the conditions of dichoptic stimulation. The waves spread over a distance that exceeds the region activated by the triggering stimulus when it is presented in isolation and propagate at speeds that are several-fold slower than propagation through horizontal connections. Therefore, these results demonstrate that under an appropriate visual context, the cortical circuitry in alert animals is capable of supporting long-range traveling waves that are triggered by local stimulation.

The dichoptic condition consisted of a stimulus sequence that in humans, reliably produces traveling waves measurable using psychophysics and brain imaging (Lee et al. 2005, 2007; Wilson et al. 2001). Moreover, this sequence produces reliable, time-locked waves in human V1, even when people are not aware of the stimulus sequence (Lee et al. 2007). Thus for our present purposes, this stimulus sequence is adequate for answering the question motivating our study: can local visual stimulation trigger long-range traveling cortical waves in V1? In asking this question, we are making no claims about what the monkeys are perceiving nor is interpretation of our results dependent on the monkeys' perceptual experiences.

We are not surprised that physical waves in the stimulus-wave condition evoked larger and more reliable modulations of activity than the activity modulations achieved in the dichoptic condition. It is unlikely that traveling waves were successfully triggered on every dichoptic trial presented to the monkeys. Indeed, comparable stimulus sequences viewed by human observers failed to generate perceptual traveling waves for a variable fraction of trials. Among three observers tested in a pilot study on multiple blocks of trials using exactly the same stimulus conditions experienced by our two monkeys, the incidence of "successful trials" (i.e., a perceptual wave was triggered and traveled the full distance of the dichoptic stimulus) ranged from 67% to 96% over blocks of trials (average success rate across observers and blocks was 87%). Hence, the traveling wave in the VSDI signals reported here is likely to be diluted by averaging across all trials, including some "failure" trials. We doubt, however, that this is the sole reason for smaller modulations to perceptual vs. physical waves. Why else might modulations in neural responses/VSDI signals be smaller on perceptual wave trials than on physical wave trials?

Percept-related modulations in V1 activity during dichoptic stimulation are typically smaller than those produced by physically changing the stimulus. From single-unit recordings, we know that the responses of only a fraction of V1 neurons correlate with perceptual fluctuations during rivalry (Keliris et al. 2010; Leopold and Logothetis 1996), whereas physical changes in stimulus contrast undoubtedly modulate the responses of virtually all V1 neurons. Moreover, among those neurons whose responses are modulated during rivalry, those modulations are not equivalent to modulations produced by physically turning the stimulus on and off. From fMRI studies in humans, too, the responses associated with perceptual modulations of rival stimulus visibility tend to be smaller than those produced by physical changes that mimic the perceptual changes [Polonsky et al. (2000); Wunderlich et al. (2005), but see Tong and Engel (2001)]. Results from psychophysical studies also point to this same conclusion: a suppressed stimulus retains some of its effectiveness, as evidenced by its ability to induce visual adaptation after-effects (Blake et al.

2006; Lehmkuhle and Fox 1975; O'Shea and Crassini 1981; Wade and Wenderoth 1978) and to alter the appearance of the currently dominant stimulus (Andrews and Blakemore 1999; Pearson and Clifford 2005). Considered together, these neurophysiological and psychophysical findings imply that dichoptic suppression, including that presumed to underlie the spatiotemporal dynamics of the traveling waves that we measured, does not involve the wholesale elimination of evoked neuronal activity.

Our results support the contention that hemodynamic measurements of stimulus-evoked activity in the visual cortex are generally consistent with neurophysiological measurements (Cardoso et al. 2012; Heeger et al. 2000). Most other studies of physiological correlates of dichoptic stimulation have focused on spontaneous fluctuations in perceptual states (see above). In the present study, however, we measured stimulus-triggered transitions, and the traveling waves that we observed with VSDI corroborate previously reported fMRI measurements of triggered traveling waves in human V1 (Lee et al. 2005, 2007).

Although we measured traveling waves of activity in V1 under conditions of dichoptic stimulation, we do not wish to imply that V1 activity fully accounts for perception of traveling waves during binocular rivalry. Indeed, there is reason to believe that V1 activity alone is insufficient for the experience of rivalry: stimulus-triggered waves of activity can be observed in V1 with fMRI even when observers are unaware of those waves, and awareness of rivalry is more closely associated with activity in extrastriate visual areas (Lee et al. 2007). Still, the presence of traveling waves in V1 implicates it as a component within a network of areas involved in rivalry, as embodied in computational models positing a hierarchy of processing stages in binocular rivalry (Blake and Logothetis 2002; Freeman 2005; Tong et al. 2006; Wilson 2003) and other bistable phenomena (Donner et al. 2008).

Our results were obtained under a specific visual context that was designed to trigger traveling waves externally and channel their path of propagation. This stimulus regime is markedly different from efforts to induce traveling waves in V1 in response to a single, isolated visual stimulation, efforts that have produced conflicting interpretations (Reynaud et al. 2012; Sato et al. 2012; Sit et al. 2009). There is a general agreement that responses to isolated, localized stimuli produce activity that extends only a few millimeters beyond the direct retinotopic representation in V1, with dynamics that are much faster than the dynamics reported here. However, there is some disagreement regarding the nature of these dynamics and the possible underlying mechanisms.

Several studies (Palmer et al. 2012; Sit et al. 2009) concluded that the spatial extent of V1 responses to a local, isolated stimulus is fully explained by the cortical point image (McIlwain 1986) that reflects the size and scatter of V1 neurons' receptive fields (Palmer et al. 2012; Van Essen et al. 1984). Quantitative analysis of VSDI measurements in fixating monkeys suggests that the responses are inconsistent with a traveling wave that starts locally and expands at a constant speed (Sit et al. 2009). Specifically, response onset was nearly instantaneous over the entire active region, whereas time to peak was shorter at the center of the active region and progressively delayed as one moved away from the center. The near-simultaneous response onset is inconsistent with a traveling wave that propagates at a constant speed through horizontal connections. These differences in the dynamics across space are better explained by spatial differences in local gain that could be implemented by a population gain-control mechanism operating simultaneously over the entire active region (Sit et al. 2009). Whereas additional research is needed to understand the nature of V1 responses to isolated, localized visual stimuli and their underlying mechanisms, the results of the current study reveal a different phenomenon that cannot be explained by local gain-control mechanisms or spread through horizontal connections. Instead, the traveling waves measured in the current study may be mediated by multisynaptic, regenerative processes that support slow propagation over relatively large distances within the retinotopic map of the visual field. Unlike the isotropic spread of waves created when a pebble is dropped into a pond, these slowly propagating traveling waves are constrained to paths defined by the existing neural activity associated with the configuration of the carrier stimulus on which those waves ride.

ACKNOWLEDGMENTS

The authors thank Sang-Hun Lee for assistance with generating the visual stimuli and members of the E. Seidemann laboratory for their contributions to this project.

GRANTS

Support for this work was provided by the National Eye Institute (Grant RO1-EY016752).

DISCLOSURES

The authors declare no competing financial interests.

AUTHOR CONTRIBUTIONS

Author contributions: Z.Y., D.J.H., R.B., and E.S. conception and design of research; Z.Y. performed experiments; Z.Y. analyzed data; Z.Y., D.J.H., R.B., and E.S. interpreted results of experiments; Z.Y. prepared figures; Z.Y., D.J.H., R.B., and E.S. drafted manuscript; Z.Y., D.J.H., R.B., and E.S. edited and revised manuscript; Z.Y., D.J.H., R.B., and E.S. approved final version of manuscript.

REFERENCES

Andrews TJ, Blakemore C. Form and motion have independent access to consciousness. *Nat Neurosci* 2: 405–406, 1999.

Bartels A, Logothetis NK, Moutoussis K. fMRI and its interpretations: an illustration on directional selectivity in area V5/MT. *Trends Neurosci* 31: 444–453, 2008.

Benucci A, Frazor RA, Carandini M. Standing waves and traveling waves distinguish two circuits in visual cortex. *Neuron* 55: 103–117, 2007.

Blake R, Logothetis NK. Visual competition. *Nat Rev Neurosci* 3: 13–23, 2002.

Blake R, Tadin D, Sobel K, Chong SC, Raissian R. Strength of early visual adaptation depends on visual awareness. *Proc Natl Acad Sci USA* 103: 4783–4788, 2006.

Cardoso MM, Sirotin YB, Lima B, Glushenkova E, Das A. The neuroimaging signal is a linear sum of neurally distinct stimulus- and task-related components. *Nat Neurosci* 15: 1298–1306, 2012.

Chen Y, Geisler WS, Seidemann E. Optimal decoding of correlated neural population responses in the primate visual cortex. *Nat Neurosci* 9: 1412–1420, 2006.

Chen Y, Geisler WS, Seidemann E. Optimal temporal decoding of V1 population responses in a reaction-time detection task. *J Neurophysiol* 99: 1366–1379, 2008.

Chen Y, Palmer CR, Seidemann E. The relationship between voltage-sensitive dye imaging signals and spiking activity of neural populations in primate V1. *J Neurophysiol* 107: 3281–3295, 2012.

Donner TH, Sagi D, Bonneh Y, Heeger DJ. Opposite neural signatures of motion-induced blindness in human dorsal and ventral visual cortex. *J Neurosci* 28: 10298–10310, 2008.

Freeman AW. Multistage model for binocular rivalry. *J Neurophysiol* 94: 4412–4420, 2005.

Grinvald A, Hildesheim R. VSDI: a new era in functional imaging of cortical dynamics. *Nat Rev Neurosci* 5: 874–885, 2004.

Grinvald A, Lieke EE, Frostig RD, Hildesheim R. Cortical point-spread function and long-range lateral interactions revealed by real-time optical imaging of macaque monkey primary visual-cortex. *J Neurosci* 14: 2545–2568, 1994.

Heeger DJ, Huk AC, Geisler WS, Albrecht DG. Spikes versus BOLD: what does neuroimaging tell us about neuronal activity? *Nat Neurosci* 3: 631–633, 2000.

Heeger DJ, Ress D. What does fMRI tell us about neuronal activity? *Nat Rev Neurosci* 3: 142–151, 2002.

Jancke D, Chavane F, Naaman S, Grinvald A. Imaging cortical correlates of illusion in early visual cortex. *Nature* 428: 423–426, 2004.

Keliris GA, Logothetis NK, Tolias AS. The role of the primary visual cortex in perceptual suppression of salient visual stimuli. *J Neurosci* 30: 12353–12365, 2010.

Lauritzen M. Reading vascular changes in brain imaging: is dendritic calcium the key? *Nat Rev Neurosci* 6: 77–85, 2005.

Lee SH, Blake R, Heeger DJ. Hierarchy of cortical responses underlying binocular rivalry. *Nat Neurosci* 10: 1048–1054, 2007.

Lee SH, Blake R, Heeger DJ. Traveling waves of activity in primary visual cortex during binocular rivalry. *Nat Neurosci* 8: 22–23, 2005.

Lehmkuhle SW, Fox R. Effect of binocular rivalry suppression on motion aftereffect. *Vision Res* 15: 855–859, 1975.

Leopold DA, Logothetis NK. Activity changes in early visual cortex reflect monkeys' percepts during binocular rivalry. *Nature* 379: 549–553, 1996.

Logothetis NK, Wandell BA. Interpreting the BOLD signal. *Annu Rev Physiol* 66: 735–769, 2004.

McIlwain JT. Point images in the visual system: new interest in an old idea. *Trends Neurosci* 9: 354–358, 1986.

Nauhaus I, Busse L, Carandini M, Ringach DL. Stimulus contrast modulates functional connectivity in visual cortex. *Nat Neurosci* 12: 70–76, 2009.

O'Shea RP, Crassini B. Interocular transfer of the motion after-effect is not reduced by binocular rivalry. *Vision Res* 21: 801–804, 1981.

Palmer CR, Chen Y, Seidemann E. Uniform spatial spread of population activity in primate parafoveal V1. *J Neurophysiol* 107: 1857–1867, 2012.

Pearson J, Clifford CW. Suppressed patterns alter vision during binocular rivalry. *Curr Biol* 15: 2142–2148, 2005.

Polonsky A, Blake R, Braun T, Heeger DJ. Neuronal activity in human primary visual cortex correlates with perception during binocular rivalry. *Nat Neurosci* 3: 1153–1159, 2000.

Reynaud A, Masson GS, Chavane F. Dynamics of local input normalization result from balanced short- and long-range intracortical interactions in area V1. *J Neurosci* 32: 12558–12569, 2012.

Sato TK, Nauhaus I, Carandini M. Traveling waves in visual cortex. *Neuron* 75: 218–229, 2012.

Shoham D, Glaser DE, Arieli A, Kenet T, Wijnbergen C, Toledo Y, Hildesheim R, Grinvald A. Imaging cortical dynamics at high spatial and temporal resolution with novel blue voltage-sensitive dyes. *Neuron* 24: 791–802, 1999.

Sirotin YB, Das A. Anticipatory haemodynamic signals in sensory cortex not predicted by local neuronal activity. *Nature* 457: 475–479, 2009.

Sit YF, Chen Y, Geisler WS, Miikkulainen R, Seidemann E. Complex dynamics of V1 population responses explained by a simple gain-control model. *Neuron* 24: 943–956, 2009.

Tong F, Engel SA. Interocular rivalry revealed in the human cortical blind-spot representation. *Nature* 411: 195–199, 2001.

Tong F, Meng M, Blake R. Neural bases of binocular rivalry. *Trends Cogn Sci* 10: 502–511, 2006.

Van Essen DC, Newsome WT, Maunsell JH. The visual field representation in striate cortex of the macaque monkey: asymmetries, anisotropies, and individual variability. *Vision Res* 24: 429–448, 1984.

Wade NJ, Wenderoth P. Influence of color and contour rivalry on magnitude of tilt aftereffect. *Vision Res* 18: 827–835, 1978.

Wilson HR. Computational evidence for a rivalry hierarchy in vision. *Proc Natl Acad Sci USA* 100: 14499–14503, 2003.

Wilson HR, Blake R, Lee SH. Dynamics of travelling waves in visual perception. *Nature* 412: 907–910, 2001.

Wolfe JM. Reversing ocular dominance and suppression in a single flash. *Vision Res* 24: 471–478, 1984.

Wunderlich K, Schneider KA, Kastner S. Neural correlates of binocular rivalry in the human lateral geniculate nucleus. *Nat Neurosci* 8: 1595–1602, 2005.

Yang Z, Heeger DJ, Seidemann E. Rapid and precise retinotopic mapping of the visual cortex obtained by voltage sensitive dye imaging in the behaving monkey. *J Neurophysiol* 98: 1002–1014, 2007.